Emerging links between Greenland ice melt, Euro-Mediterranean heat extremes, and destructive convective storms

Juan Jesús González-Alemán (1), Marilena Oltmanns (2,3,4), Sergi González-Herrero (5), Frédéric Vitart (6), Markus G. Donat (7,8), Francisco Doblas-Reyes (7,8), David Barriopedro (9), Jacopo Riboldi (10), Carlos Calvo-Sancho (11), Bernat Jiménez-Esteve (9), Pep Cos (7) and Michael F. Wehner (12).

(1) AEMET/Spanish State Meteorological Agency, Madrid, Spain
(2) Alfred Wegener Institute, Bremerhaven, Germany
(3) University of Bremen, Bremen, Germany
(4) National Oceanography Centre, Southampton, UK
(5) WSL Institute for the Snow and Avalanche Research (SLF), Switzerland
(6) European Centre for Medium-Range Weather Forecasts, United Kingdom
(7) Barcelona Supercomputing Centre, Barcelona, Spain
(8) Catalan Institution for Research and Advanced Studies (ICREA), Barcelona, Spain
(9) Instituto de Geociencias (IGEO), Consejo Superior de Investigaciones Científicas - Universidad Complutense de Madrid (CSIC - UCM), Madrid, Spain
(10) Institute for Atmospheric and Climate Science, ETH Zurich, Zurich, Switzerland
(11) Centro de Investigaciones sobre Desertificación, Consejo Superior de Investigaciones Científicas (CIDE, CSIC-UV-GVA), Climate, Atmosphere and Ocean Laboratory (Climatoc-Lab), Moncada, Valencia, Spain
(12) Applied Mathematics and Computational Science Division, Lawrence Berkeley National Laboratory, Berkeley, California 94720 USA

Abstract

Greenland ice loss is accelerating, but its consequences beyond sea-level rise remain poorly understood. At the same time, the Euro-Mediterranean region is facing unprecedented summer climate extremes where the underlying mechanisms have been long debated. Here we present the first evidence of a far-reaching cascading mechanism by which Greenland ice sheet melting acts as a major forcing of hemispheric-scale, spring-summer atmospheric circulation shifts with potential high-impact effects. This has already exacerbated record-breaking and catastrophic western Euro-Mediterranean climate events, and has taken part in its accelerated warming trend relative to the global mean. Using reanalysis data, a high-resolution climate model ensemble, and process-based diagnostics, we demonstrate that these processes have contributed to recent European atmospheric heatwaves with severe socioeconomic and human impacts, marine heatwaves causing mass mortality events, and extreme convective storms such as the historic Mediterranean derecho that led to serious destruction and loss of human lives. These links situate the mechanism within the broader Earth system and points out anthropogenic climate change as a likely forcing, suggesting that cascading impacts will intensify as ice loss accelerates. We also find that CMIP6 models cannot simulate the cascading mechanism, most likely because of their inability to simulate

localised freshwater influx correctly, thus indicating that current projections of future climate may be underestimating these impacts. Our findings thus point out Greenland melting as a previously unreported major driver of spring-summer large-scale circulation changes, with potential for a systemic amplification of long-range regional climate hazards. These hazards include confirmed profound socioeconomic, human and ecological consequences with unforeseeable future effects. Thus, incorporating these processes is essential for forecasts systems, Earth system models, and long-term projections, posing a significant gap in our ability to project future risk and representing a major step towards effective early-warning and mitigation strategies.

Main

On 17 August 2022, the western Mediterranean experienced exceptionally unstable atmospheric conditions combined with pronounced wind shear. These conditions, occurring ahead of an eastward-moving trough, led to the formation of a bow-shaped system of thunderstorms. This mesoscale system produced a long path of severe winds (> 25 m s^{-1}), stretching from the Balearic Islands to the southern Czech Republic on 18 August. The strongest wind gust was recorded in Corsica, reaching 62.2 m s^{-1}, breaking numerous regional records and resulting in 12 fatalities, and 106 injured persons during the event (**González-Alemán et al. 2023**). The system was classified as a derecho (**ESSL, 2022**), a rare type of long-lasting, highly impactful and severe windstorm generated by a line of convective storms (**Johns and Hirt, 1987; Corfidi et al., 2016**), which is extremely uncommon over the Mediterranean (**Fery and Faranda, 2024**; **Surowiecki et al., 2024)**. Despite the latter, this event surprisingly ranked among the most intense derechos recorded in the world (**Li et al., 2025**).

A climate attribution exercise concluded that anthropogenic climate change (ACC) contributed to triggering the derecho (**González-Aleman et al., 2023**). **González-Aleman et al. (2023)** linked the derecho development to a simultaneous record-breaking marine heatwave (MHW) that peaked in July, with sea surface temperatures (SSTs) exceeding 3 °C above normal levels (**see Fig. 1a**) and ranking first among all years since, at least, 1940. These conditions created an environment highly favorable for extreme convective stormsHigh SSTs enhance atmospheric moisture availability and instability, providing an environment with more available potential energy for convective storms (**Trapp et al., 2007; Hoogewind et al., 2017; Battaglioli et al., 2023; Martín et al., 2024**).

The 2022 extreme MHW is consistent with the reported overall increasing trend in frequency, duration, and intensity of MHWs, based on both observational data (**Oliver et al., 2018**) and climate model simulations (**Frölicher et al., 2018; Oliver et al., 2019**). It was preceded by extraordinary atmospheric conditions in spring-summer (**Trigo et al. 2025**), with recurrent high-pressure systems, which contributed to a strong signature in the May-July atmospheric circulation field (**Fig. 1b**). This led to exceptional temperature anomalies (**Tejedor et al., 2024; Serrano-Notivoli et al., 2024**), prolonged drought conditions (**Garrido-Pérez et al. 2024**), and noteworthy human and socioeconomic impacts (**Ballester et al., 2023; Kotz et al., 2024**) over western Mediterranean countries. These extreme heating and drought conditions were partly attributed to ACC (**Faranda et al. 2023; Feser et al. 2024)**.

The concurrence of extreme atmospheric and sea surface anomalies observed in summer 2022 raises questions about large-scale drivers causing extreme-storm preconditioning environments in the Mediterranean. One potential mechanism involves dynamic teleconnections arising from subpolar North Atlantic freshwater anomalies associated with glacial and sea ice melt. The influence of ACC on ice melting has sparked much attention over the last decade. Recent research suggests that these freshwater inputs can modulate summer atmospheric circulation over Europe (**Oltmans et al. 2020; 2024; Chevuturi et al. 2025**). While winter Arctic-midlatitude linkages have been more thoroughly examined, particularly those connecting sea ice reduction and Arctic amplification to weakened zonal winds and increased planetary wave amplitude (**Francis and Vavrus, 2012; Screen and Simmonds, 2013**), their spring-to-summer counterparts remain comparatively understudied (**Coumou et al., 2018**). And there is still an overall low confidence in the relative contribution of Arctic warming to mid-latitude atmospheric changes compared to other drivers (**IPCC, 2021; Screen et al., 2018; Cohen et al., 2020; Smith et al., 2018; Blackport et al., 2021**).

To disentangle the causes for the atmospheric circulation to develop this kind of extreme behaviour in the atmospheric flow regimes, here we present a novel and comprehensive understanding of their preconditioning. Using state-of-the-art atmospheric reanalysis and climate model simulations, we propose a new cascade mechanism linking sub-Arctic Greenland melting to past European extreme atmospheric and marine HWs with catastrophic impacts, destructive and outlier-like convective storms, and which also explain their current increasing likelihood of occurrence. We argue that the deadly 2022 derecho developed as result of a cascade of processes initiated by Greenland ice melting. Our analysis also brings noteworthy implications for the understanding of the atmospheric circulation response to ACC, and discusses possible improvements in climate modelling, prediction, and projections.

Spring-summer 2022 in the context of a changing atmospheric circulation

The atmospheric circulation in spring-summer (May-to-July) 2022 was characterized by a prevalent and intense ridge activity over western Europe (**Fig. 1b-c**). This atmospheric pattern was responsible for the record-breaking and long-lasting MHWs that developed over the western Mediterranean Sea (**Fig. 1b-d**), as suggested by the statistical correlation between the upper-level geopotential height and the SSTs during the whole event (**Extended Data Fig. 1**). This association is well explained through physical processes, involving wind, sea surface evaporation, downward solar radiation, and clouds during high-pressure systems (see also **Sousa et al., 2018**). High tropospheric geopotential height (GH) anomalies cause low wind activity, which lead to low evaporative cooling in the region. Also, high pressure systems cause a decrease in cloud cover, which in turn leads to more solar radiation reaching the surface and heating it.

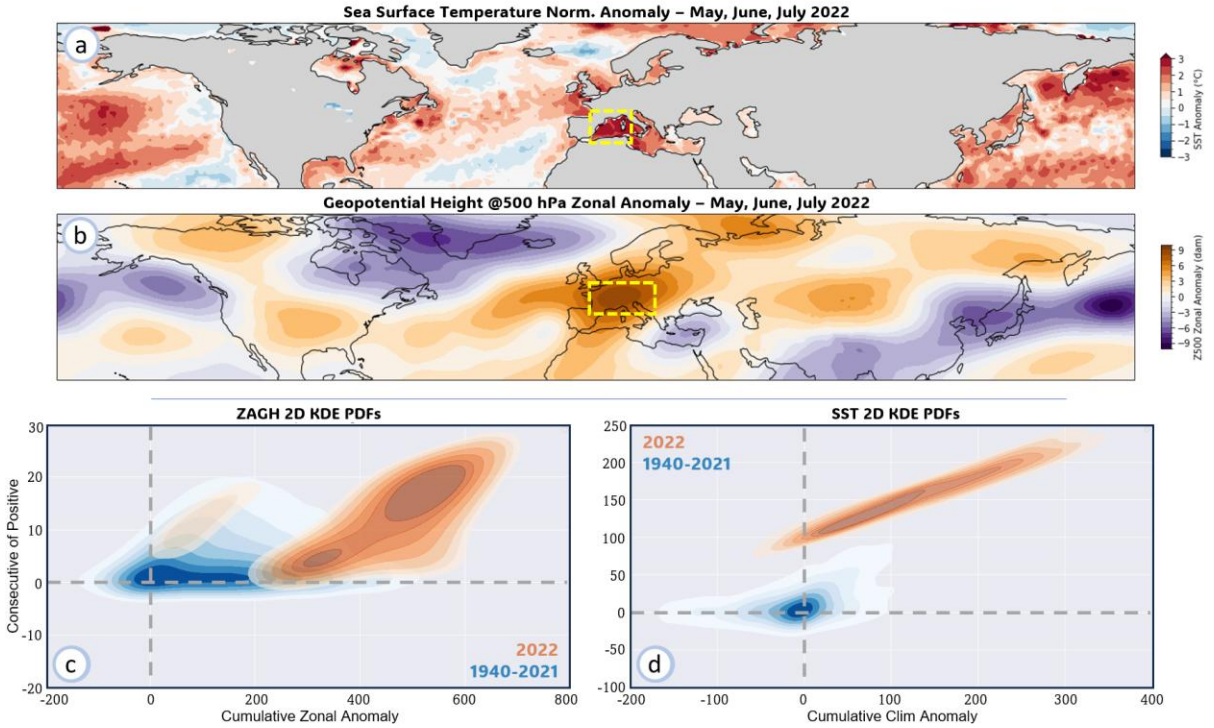

Fig. 1. Extreme atmospheric and sea conditions over the western Mediterranean in 2022. (a) Average (MJJ) of the sea surface temperature anomaly. (b) Average (MJJ) of the zonal anomaly of geopotential height at 500 hPa (ZAGH). (c) 2D probability density functions for ZAGH daily time series over the yellow box in (b), with respect to its cumulative anomaly (x-axis) and its number of consecutive positive values (y-axis). (d) Same as (c) but for SSTs over the yellow box in (a). Data from ERA5 reanalysis.

The atmospheric circulation in spring-summer 2022 can be placed well in the context of its observed changes over the last decades. Over the last 30 years (1993-2022), Europe experienced an increase in the frequency of positive GH zonal anomalies at 500 hPa (ZAGH), i.e. high pressure ridges, compared to the first 30 years of the considered period (1950-1979) (**Fig. 2a**). This suggests changes in the circulation's dynamics over the region -and not only thermodynamic- since we consider zonal anomalies (longitude-wise) instead of climatological ones (time-wise). In addition to the shift in the mean ZAGH, there is an even more worth-mentioning increase of the variability (std), which indicates more extreme situations. As in the ZAGH, remarkable non-linear changes between the two distributions appear in the western Mediterranean SSTs (**Fig. 2b)**, mostly affecting the shape of the right tail.

To assess whether these changes are specific to western Europe or part of broader hemispheric changes in the general atmospheric circulation, we divided the whole Northern Hemisphere in regular 5ºx5º boxes and repeated the analysis for each of them. The results (**Fig. 2c**) indicate widespread changes in dynamics, with the western Mediterranean being a hotspot with the largest positive differences (shifting area between the distributions). These anomalies seem to be associated with a Rossby wave pattern initiated over the North Atlantic and vanishing over the Middle East, as indicated by the correlation analysis in **Fig. 2d**. Thus, we next search for a plausible mechanism that explains such a wave-like pattern.

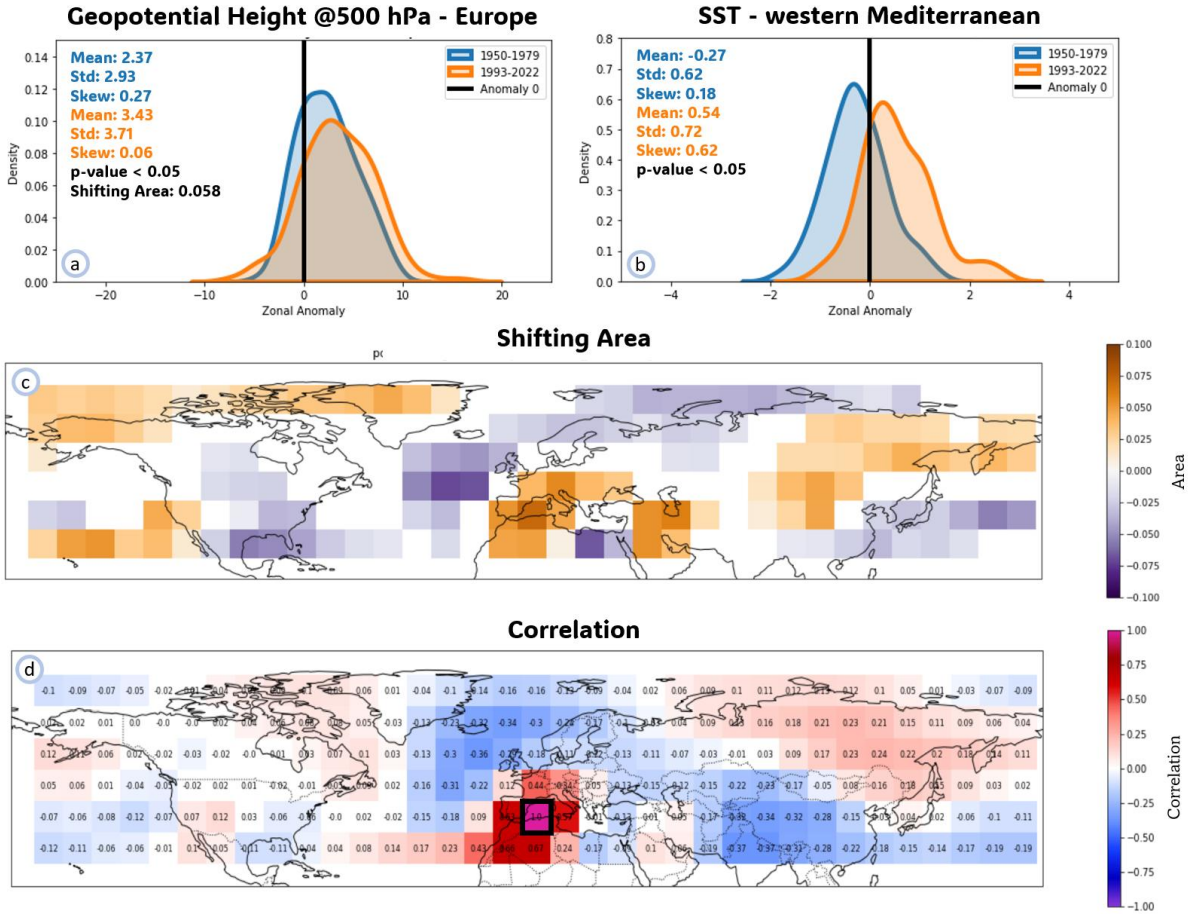

Fig. 2: Changes in the geopotential height anomalies over the last decades. (a-b) Probability density functions of (a) April-to-August monthly ZAGH over the yellow box in Fig. 1b and (b) SST over the yellow box in Fig. 1a. (c) Spatial distribution of the shifting area between the two density functions as in (a) –where ZAGH ≥ 0– calculated for each 5ºx5º deg. boxes. (d) Temporal Person's correlation of monthly values of ZAGH between each 5ºx5º box and the black box (only boxes with p-value ≥ 0.05 are coloured). Data from ERA5 reanalysis.

Links between North Atlantic SST and European atmospheric circulation

We consider two different atmospheric circulation states over western Europe in spring-summer, characterized by years with high and years with low persistence and/or intensity in ridge activity [high ridge activity (HRA); low ridge activity (LRA)] over western Europe. HRA years have ≥ 3 months –within the period of April-August– with ≥ 5 dam in ZAGH and LRA years have ≥2 months below 0 dam (**Fig. 2a; see Methods and Extended Data Fig. 2**). We find that these two groups display opposite SST patterns over the North Atlantic (**Fig. 3a,b**): HRA years are characterized by an enhanced midlatitude SST gradient east of Newfoundland, with anomalously cold SSTs to the north in the subpolar North Atlantic, and anomalously warm SSTs to the south, more marked over the western North Atlantic. This pattern is consistent with that of 2022, although with slight changes, e.g., a similar warm-cold-warm tripole but with the southern warm anomaly being further north in 2022. During LRA years, the SST gradient over the same region is reduced, with warm SST anomalies to the north and cold SST anomalies to the south.

The SST pattern in HRA years features enhanced baroclinicity over the western North Atlantic (**Fig. 3a)**, which favors cyclonic activity over the northeastern Atlantic and ridge building over western Europe (**Fig. 3c**). The opposite behaviour is seen in LRA (**Fig. 3b-d**). The link between cyclonic activity in the northeastern Atlantic and ridging over western Europe is supported by well-known physical processes involving dry (**e.g., Colucci 1985, Nakamura and Wallace 1993**) and moist dynamics (**Pfahl et al. 2015**). The ridge in HRA years appears to be part of quasi-stationary and amplified Rossby wave blocked pattern, as indicated by the anomalously strong convergence of wave-activity flux (**Nakamura et al. 1997**) to the west of the ridge (**Fig. 3c)**. Conversely, given the stationarity of the pattern, the contribution from transient recurrent Rossby wave packets (**e.g., Röthlisberger et al. 2019**) can be ruled out for this case (**see Supplementary Information and Extended Data Fig. 4**). Moist processes, on the other hand, can affect the large-scale circulation through latent heat release: its occurrence results in negative upper-tropospheric (potential) vorticity anomalies that intensify upper-level ridges and act to maintain high GH (**Steinfeld et al. 2019, Wandel et al. 2024**). The contribution of moist processes is visible in HRA by the stronger than normal warm and humid air advection coupled with upper-level divergence and warm conveyor belt (WCB; **Pfahl et al. 2015**) activity to the west of the ridge, indicating the occurrence of anomalously strong latent heating thereby (**Fig. 3e-h**). This does not occur in LRA. We are then able to close the chain of processes of the atmospheric branch: the enhanced SST gradient leads to a higher than usual baroclinicity over the western Atlantic that results in enhanced cyclonic activity, which in turn supports the seasonal persistence of positive ZAGH over western Europe in HRA years. These findings in the synoptic dynamics associated with HRA years are thus consistent with the wave-like signal observed in **Fig. 2c**, as HRA years are responsible for the increase in the mean and upper extreme in 1993-2022 wrt. 1950-1979 (**Fig. 2b**).

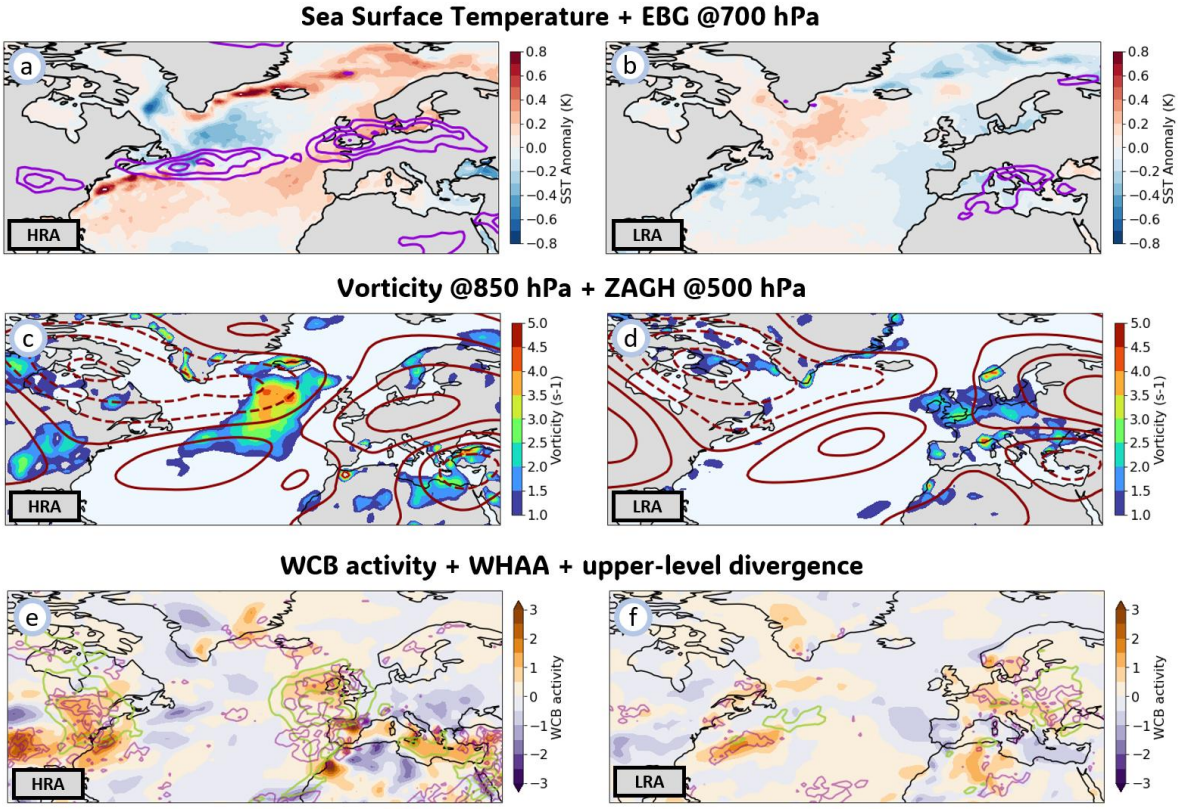

Fig. 3: Ridge building from synoptic-scale dynamical processes connected to sea surface temperature conditions in the North Atlantic. (a-b) MJJ sea surface temperature (shaded) and positive Eady baroclinic growth (EBG; contours; interval 0.1x10^1 s^{-1}) for (a) HRA and (b) LRA years. (c-d) MJJ 850 hPa vorticity (shaded) and ZAGH (contours; interval 2 dam) for (c) HRA and (d) LRA years. (e-f) MJJ WCB activity proxy (shaded), 850 hPa equivalent potential temperature advection (warm and humid air advection, WHAA; green contours; 0.5x10^5 K s^{-1}) and upper-level (150-300 hPa) divergence (violet contours; 0.25x10^6 s^{-1}) for (e) HRA and (f) LRA years. The statistical significance analysis for this panel is shown in **Extended Data Fig. 3**.

Surface impacts of the European persistent atmospheric circulation conditions

The steady atmospheric circulation conditions revealed herein have a remarkable surface footprint. The impact of the persistent western Europe ridge building (HRA years) on the western Euro-Mediterranean warming is demonstrated in **Fig. 4a**. An opposite behaviour is seen in LRA (**Fig. 4b**), with anomalously cold SSTs accompanying weak ridging. This is also supported by the correlation matrix in **Extended Data Fig. 1**, showing strong climatological links between GH and SST. Note also that HRA years are those responsible for the different warm tail behaviour of the SST distribution in the 1993-2022 period (**Fig. 2b**), mainly associated with 2003, 2015 and 2022 extreme marine HWs (**Extended Data Fig. 5b).** A similar signal is obtained for atmospheric HWs, with HRA causing more frequent and larger-magnitude events, just over western Europe (**Extended Data Fig. 5a**).

Results so far point toward a far-reaching atmospheric bridge involving different processes such as SST gradient strengthening, cyclone activity, ridge building and extreme and persistent

surface atmospheric and marine heating. However, this atmospheric bridge has another noteworthy surface consequence: the HRA group is also associated with a more favourable environment for extreme high-impact convective storm development, probably linked to the marine warming in the western Mediterranean. This is reflected by more (p-value < 0.01) intense convective precipitation (**Fig. 4c**), stronger convective wind gusts (**Fig. 4d**) and higher values of convective hazard indices (**Taszarek et al., 2021; see Methods**) during HRA years (**Fig. 4e-j)**, particularly in their upper values.

Connections with Greenland ice sheet melting

Recent studies have identified links between the large-scale atmospheric circulation over Europe and the preceding wintertime North Atlantic SSTs (**Duchez et al., 2016; Mecking et al., 2019; Krüger et al., 2023; Oltmanns et al., 2024**) and surface freshwater from melting (**Oltmanns et al., 2024; Chevuturi et al., 2025**). Consistent with these findings, our composite analysis reveals that prior to the spring-summers of HRA, the late winter-spring SST in the southern subpolar North Atlantic is reduced relative to the years with LRA (**Fig. 4k**). The relatively colder SST is, in turn, linked to a reduced sea surface salinity (SSS) (**Fig. 4m**), corresponding to enhanced surface freshening.

Enhanced surface cooling and freshening rates are observed from the previous autumn and winter during HRA (**Fig. 4l and 4n**). In these seasons, the subpolar SST tends to be warmer than the air aloft. Enhanced surface freshening increases the stratification of the ocean, causing a faster adjustment of the SST to the lower air temperatures due to reduced downward propagation of the cooling to deeper levels. Large freshwater anomalies can thus lead to cold subpolar SST anomalies at the surface in winter (**Oltmanns et al., 2020; 2024**). We therefore attribute the enhanced cooling rates and subpolar cold anomalies to freshwater.

Moreover, the spatial distribution and seasonality of the enhanced freshening rate in autumn (**Fig. 4m**), leading to the cold anomaly in winter (**Fig. 4n**) have previously been identified as a typical signature of melt- or runoff-driven freshwater anomalies (**Oltmanns et al., 2024; in revision**). Runoff-driven cold anomalies are strongest over the southeast subpolar gyre where the climatological surface heat fluxes are weaker and where the ocean surface mixed layers are shallower. In contrast, over the west subpolar gyre, the climatological surface heat losses are stronger and erode a stratified freshwater layer. The competition between the destabilising surface heat losses and the stabilising surface freshening gives the cold anomalies over the southeastern subpolar North Atlantic their characteristic shape, location and comparatively shallow downwards extent (**Oltmanns et al., 2024**).

The link between the cold wintertime SST anomalies in the south subpolar North Atlantic and preceding summer melting is further supported by Greenland runoff data since 1950, obtained from the Greenland climate model MAR (**Fettweis, 2022**). In the years prior to the subpolar cold anomaly (and HRA) years, the runoff from Greenland was on average 81.6 Gt larger than prior to the subpolar warm anomaly (and LRA) years (p-value = 0.01).

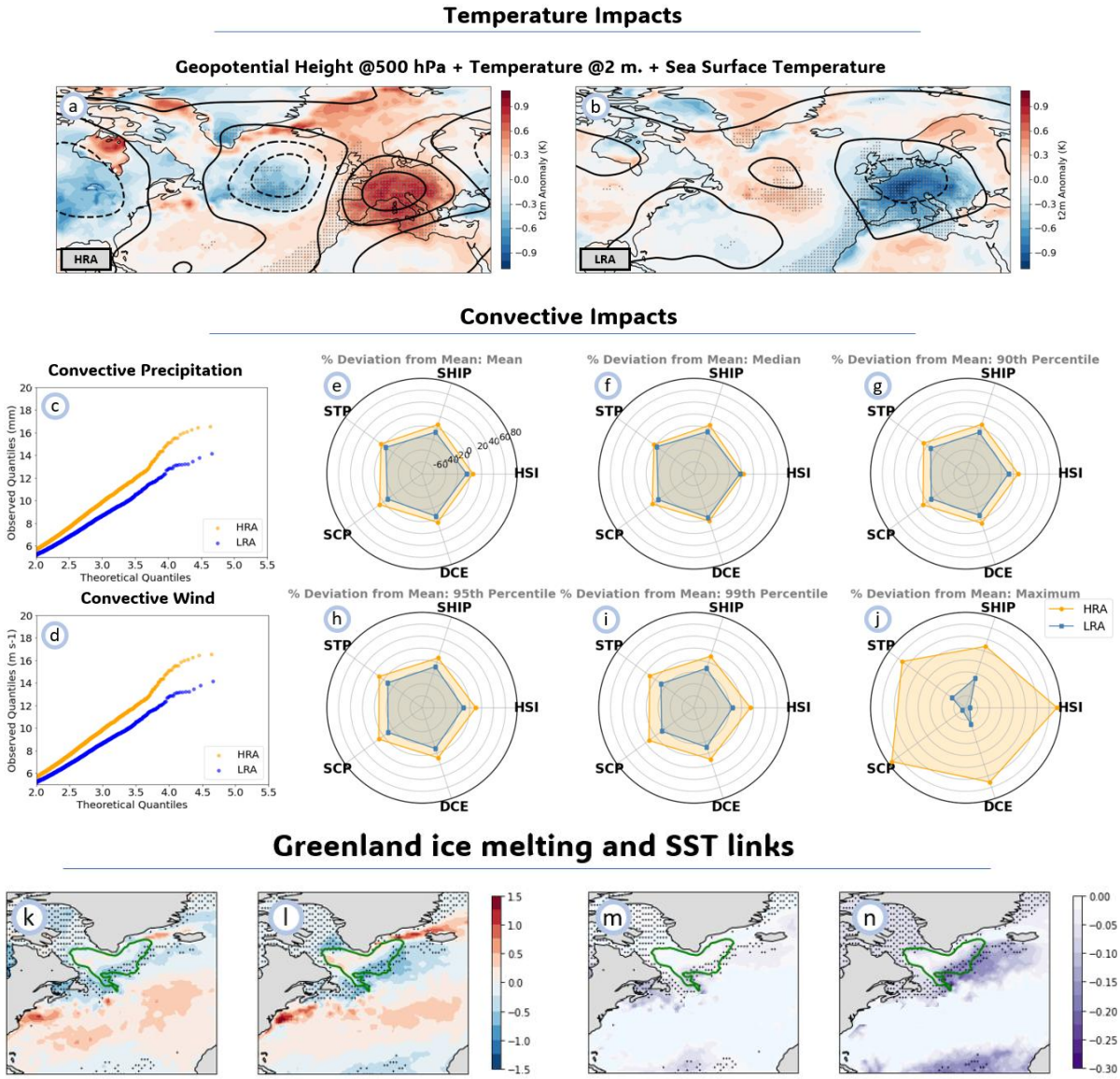

Fig. 4: Surface impacts of the cascading mechanism and its triggering source. (a-b) Composite anomaly of 500 hPa geopotential height for 1950-2022 (MJJ; black contours; interval 2 dam) and sea surface temperature (JA; sea regions) and 2-meters temperature (JA; land regions) (shaded) for (a) HRA (b) LRA years. (c-d) Quantile-quantile plots of convective precipitation and convective wind over the western Mediterranean for HRA (orange) and LRA (blue) years in JA. (e-j) Statistical metrics in environmental proxies for convective activity's hazard potential (see Methods) for HRA and LRA years in JA. (k,m) Composite March differences of (k) sea surface temperature (SST) and (m) sea surface salinity (SSS) between HRA and LRA years. (l,n) Composite differences of the seasonal surface cooling (l) and surface freshening (n) between the HRA and LRA years, with negative SSS anomalies indicating enhanced freshening. The seasonal cooling and freshening refers to the SST and SSS differences from autumn (averaged over September to November) to March. The SSS has been estimated using a surface mass balance (See Methods). The green contour line represents the mean location of the subpolar gyre, represented by the -0.5 m isoline of the mean absolute dynamic topography. Dots indicate significant statistical difference ($p \leq 0.05$; rank-sum test).

Physics-based support: The link between subpolar gyre and atmospheric circulation in climate models

So far our analysis has been based on reanalysis data. To test whether the causal links inferred from composite analyses represents a plausible physical mechanism, we conducted model simulations with the Integrated Forecast System (IFS; **Molteni et al, 1996**), the global atmospheric model from the European Centre for Medium Range Weather Forecasts (ECMWF). We ran the model in ensemble mode with 25 members, from the 1st of May 2022 at 00 UTC. The model response to the observed SSTs as boundary conditions is consistent with the atmospheric behavior over Europe in spring-summer 2022. The model produces an increase in the likelihood (proportion of ensemble members) and/or magnitude of ridge building over western-central Europe (**Fig. 5a,b)** with respect to the model's response to climatological SSTs. However, intrinsic model errors are considerable as we go backward in the initialisation time (e.g. March initialization, not shown). It is also to note the remarkably different signal by model simulations, as horizontal grid resolution is important for the correct modelling of moist synoptic-scale processes like extratropical cyclones and their accompanying WCB dynamics (**Priestley and Catto, 2022**).

We also run the model again using the SST pattern in HRA years, but from the 1st of March to leave time for the model to spin up (i.e., the model initial adjustment time to reach realistic atmospheric conditions). Again, the response is remarkably similar to observations **(Fig. 5c,d)**, not only in the western Europe ridging but also in other key atmospheric structure changes (see **Supplementary Information**). These results indicate that the causal links between subpolar SSTs and the European atmospheric circulation can be thus regarded as a physically-consistent mechanism.

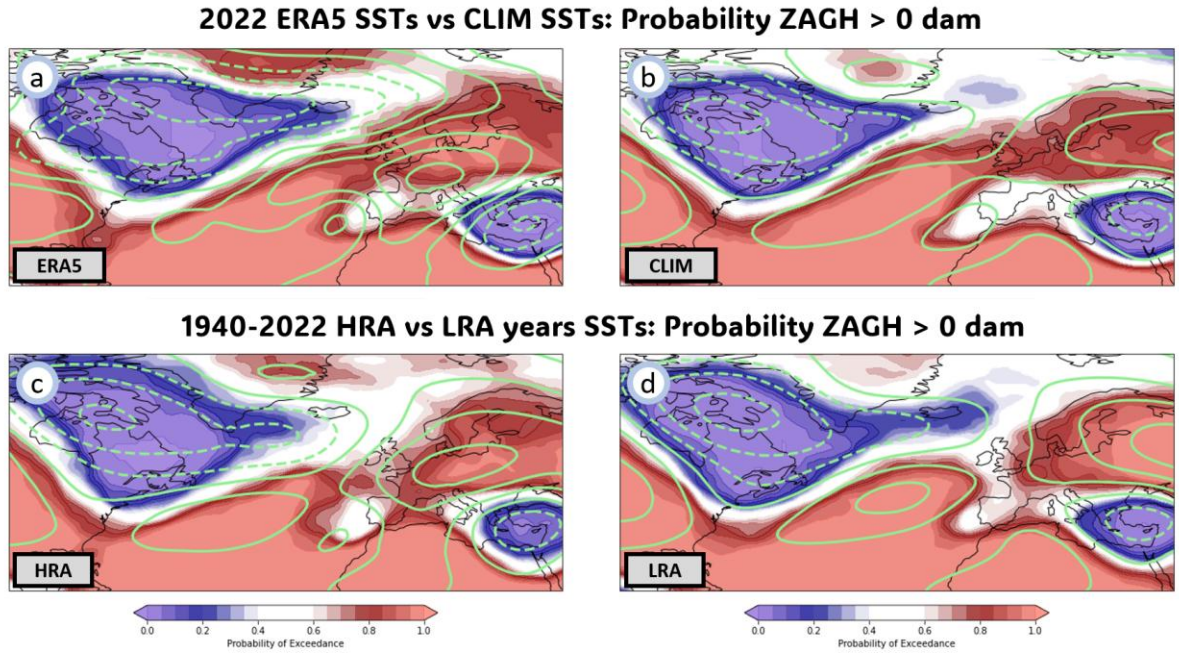

Fig. 5: Climate model simulations support European atmospheric circulation conditions relationship to North Atlantic sea surface temperature patterns. (a-b) Probability of zonal anomaly of geopotential height (ZAGH) ≥ 0 by the ECMWF-IFS ensemble simulations with

prescribed SSTs initialized on 1st of May at 00 UTC for MJJ with (a) observed SSTs and (b) ERA5 climatological SSTs. (c-d) The same as in (a-b) but with the prescribed SST composites from (c) HRA and (d) LRA years and initialized on 1st of March at 00 UTC. In green contours, the observed ZAGH (green contours; interval 2 dam) for each case (a: MJJ 2022; b: MJJ 1950-2022; c: MJJ HRA years; d: MJJ LRA years) field is represented for better comparison purposes.

Implications for climate predictability

Here we introduce a novel cascading mechanism which involves different phenomena within the Earth system. We provide evidence of a far-reaching atmospheric bridge that ultimately connects the freshening of sub-polar Atlantic waters driven by summer ice sheet melting in Greenland with the intensification of severe heatwaves and convective events in the western Euro-Mediterranean via mid-latitude dynamics. Increased ice melt contributes to stronger North Atlantic SST gradients, enhancing baroclinicity and promoting cyclonic formation, which fosters downstream ridge building over western Europe. The persistent anticyclonic conditions impact on the surface as extreme and long-lasting atmospheric and marine HWs, and finally, adapting the environment for the development of extreme convective storms, through high moisture and heat availability. This mechanism is illustrated in **Fig. 6**.

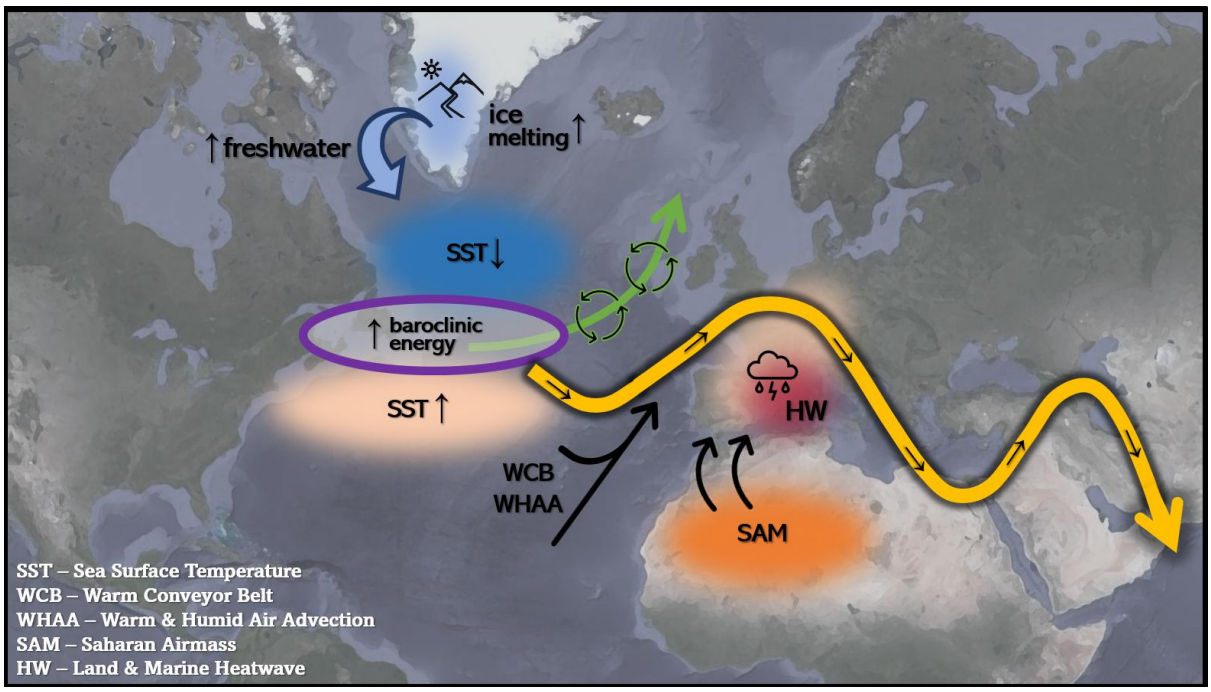

Fig. 6: Illustrative scheme summarizing the cascading mechanism. Freshwater influx from ice melting in the Greenland ice sheet cools North Atlantic subpolar surface waters (SST) locally, enhancing baroclinic energy and fostering jet stream meanders due to extratropical cyclogenesis. Cyclones favor the advection of vorticity and warm, humid air (WHAA) through the development of warm conveyor belts (WCB), which provokes ridge building downstream. Persistent ridge building induces atmospheric and marine heatwave (HW) formation and subsequent extreme and impactful convective storms over the western Mediterranean. In this cascade of events, the Saharan Airmass (SAM) is forced to move towards the north, which indicates that the process of persistent and/or amplified ridge building caused by the extratropical cyclones tends to be accompanied by (or

facilitates) a northward elongation of the North Africa subtropical ridge and its associated over-heated air.

Our results thus suggest that years with extreme Greenland melting and runoff trigger more extreme heat and convective activity over western Euro-Mediterranean. The record-breaking and destructive Mediterranean derecho windstorm in summer 2022, extreme atmospheric and marine HWs and the large-scale conditions in that year, can be then regarded as developed under this cascading mechanism. Another rare and convective storm with deadly giant hail developed in summer 2022 under the same conditions (**Martin et al., 2024**). Other years contributing to HRA have also recorded severe convective storms over the western Mediterranean basin, whose characteristics were outlier-like (e.g. the derecho in August 2003; **López et al. 2007; see Supplementary Information**). HWs with fatal societal impacts have also developed in HRA years, like in 2003, 2015 and 2017 (e.g. **Sánchez-Benítez et al. 2018**). In addition to the resulting societal and human impacts, the proposed mechanism would also entail enormous marine ecological impacts in the Mediterranean, like widespread mass mortality events, as reported by **Garrabout et al. (2022)** with recent MHWs. These latter impacts posed an unprecedented threat to ecosystems' health and functioning.

The proposed mechanism helps to explain spring-summer year-to-year variations of the climate evolution over Europe and therefore represents a potential source of predictability for summer seasonal forecasting **(Torralba et al., 2024; Patterson et al., 2024)**, as it involves a sequence of events that can be traced back a year in advance. Thus, we argue that monitoring previous summer ice melting and winter-spring subpolar SSTs in the North Atlantic would be key to predicting subsequent summer extremes in both atmospheric and marine HWs and extreme behaviour of convective storms over the western Euro-Mediterranean.

Results from this work are consistent with recent literature. Several studies [e.g. **Bischof et al. (2023); Kim et al. (2024); Yin et al. (2024); Christ et al. (2025)**] have pointed out the role of North Atlantic SSTs on the downstream development of atmospheric ridges and heatwaves over Europe, while the subpolar North Atlantic freshwater has been suggested to be a key driver of the summer mid-latitude climate variability in Europe (**Oltmanns et al., 2020; Oltmanns et al., 2024; Ma et al., 2024; Chevuturi et al., 2025; Grist et al., 2025**). Our analysis is also in line with the reported increase in summer cyclonic activity over the Eastern North Atlantic (**D'Andrea et al., 2024)** and the increasing frequency of subtropical ridges (**Sousa et al., 2021; see Supplementary Information**), which has been recently linked to Mediterranean summer marine heatwaves (**Pastor et al., 2024; Bonino et al. 2025**). Also, as Saharan air intrusions (SAIs) are often connected to subtropical ridges and temperature extremes over the western Mediterranean (**Sousa et al. 2019; Cos et al, 2025),** an analysis of the relationship between SAIs and the proposed mechanism has been addressed. The analysis indicates that more SAIs come into action during HRA year, likely incorporating non-linear effects, i.e., modulating the ridge building response to extratropical cyclones (**see Supplementary Information**), and probably helping to also explain the really extreme tail behaviour of SSTs in **Fig. 2b**. Therefore, the chain of cascading processes described herein robustly provides a potential explanation for the increased ridging over Europe, and points to Greenland ice sheet melting as an unreported

driver of summer Mediterranean climate dynamics. While several of the individual processes contributing to the mechanism described herein have been recently noted in the literature, this study provides a more holistic perspective, integrating them into a fully articulated cascading mechanism that also reveals new and noteworthy surface impacts such as extreme (atmospheric and marine) HWs and convective storms.

Implications for climate modelling and projections

While the melting of the Greenland ice sheet is characterised by substantial interannual variability (**Trusel et al., 2018)**, linked to the summer atmospheric circulation (**Välisuo et al., 2018**), it has also experienced a noticeable increase over the last decades and is expected to further increase in a warming climate (**Trusel et al., 2018; Hanna et al., 2021; Zhang et al., 2025**). The amplified long term post-industrial polar warming (**Cohen et al., 2014**) and melting trend **(Trusel et al., 2018)** is forced by greenhouse gas emissions, leading to increased freshwater discharges into the North Atlantic. Consistent with the increasing greenhouse gas emissions, Greenland melting, and North Atlantic freshening, there is a significant cooling (or reduced warming) trend over the southeastern subpolar North Atlantic. This cold anomaly is often referred to as the North Atlantic cold blob or warming hole and connected to a decline of the large-scale Atlantic Meridional Overturning Circulation (AMOC, **Caesar et al., 2018**). The AMOC decline is another implication of the increased freshening, as the freshwater simultaneously drives a localised surface cooling and prevents warm, subtropical waters from reaching north (**Jackson et al., 2023; Pontes and Menviel, 2024**). Considering these facts and that the spatial characteristics of the North Atlantic cold blob strongly resemble the cold and fresh anomalies found in HRA years (**Extended Data Fig. 6**), the proposed cascading chain of events will likely be reinforced under enhanced ACC. Favourable conditions for more frequent, more intense and potentially devastating Euro-Mediterranean HWs and convective storms are then expected over the coming decades.

We therefore propose that, despite the plausibility of the mechanism being a result of internal climate variability, external forcing like ACC potentially contributes to the cascading chain of events. ACC likely magnifies the severity of the events and/or facilitates the triggering mechanisms (see e.g. the post-1990 increase in HRA years in **Extended Data Fig. 2**), ultimately enhancing the risk from HWs and convective storm hazards (see more in **Supplementary Information**). While the link between ACC and extreme severe convective storms has been debated (**IPCC, 2021**), being historically difficult to establish due to limited observational records and complex dynamics, recent advances have started to close this gap (see **Supplementary Information**), and our results incorporate a dynamical mechanism for this connection.

To assess possible influences of ACC in the cascading processes, we undertake an assessment of (53) models from the Coupled Model Intercomparison 6 (CMIP6). If the cascading processes evident in observations were partially forced by ACC and also present in the models, we would expect some changes in ZAGH. However, despite the strong and robust signal emerging in observations, all the models struggle to reproduce the observed changes in the ZAGH

distributions (**Fig. 2a**), including the shift in the mean, increase in variability and changing tails (**Extended Data Fig. 7**). One possible explanation for this discrepancy is a possible influence by internal climate variability in the mechanism triggering, but it is to note that these models incorporate the strong melting trends of recent decades. Another stronger possibility is that the key processes in the observed mechanisms are not fully captured by these models, due to missing processes and/or coarse spatial resolution (**Schmidt et al., 2025**). If this is the case, current historical simulations and future projections may underestimate the impact of ice melting on extreme warming and convective risks over western Europe (see more in **Supplementary Information**). Key processes in the proposed mechanism include the increased freshwater discharge from melting ice sheets and glaciers, the reduced vertical mixing in the subpolar North Atlantic, and the subsequent surface cooling of subpolar SST in the North Atlantic. According to this, an adequate representation of the processes, relevant for the freshening of the subpolar Atlantic, would be critical for capturing the proposed cascading mechanism in climate simulations. Many climate models have difficulties in simulating the ice-ocean-atmosphere coupling and adequately representing the freshwater flux from melting (**Schmidt et al. 2025**). This is due to an insufficient resolution to resolve the mixing processes in the subpolar North Atlantic and a lack of interactive ice-sheet models (**Roberts et al., 2025**), leading to freshwater biases in the North Atlantic (**van Westen and Dijkstra, 2024**). The use of strong numerical diffusion, which tends to dampen SST gradients (**Moreno-Chamarro et al. 2022**) and models' difficulties to simulate the warming hole (**Fan et al. 2024**) are other potential reasons. Moreover, additional sources of model biases may involve the misrepresentation of synoptic and cyclone dynamics because of their coarse resolution (**Priestley et al., 2020; Priestley and Catto, 2022**). Without explicitly accounting for these processes, models will not be able to capture the full chain of interactions described here.

Better understanding of atmospheric circulation changes

This work also provides valuable insight on a current topic of high interest in the field. western Europe is under an accelerated heatwave trend, warming in boreal summer about triple the global mean since 1980, being identified as a heatwave spot (**van Oldenborgh et al., 2009; Rousi et al., 2022; Twardosz et al., 2021; Vautard et al. 2023; Yin et al. 2024; Dong et al. 2024**). This differential heating in Europe has sparked a vibrant debate over the last years in the community, where different contributing processes have been proposed (**see Supplementary Information**). The analysis undertaken here indicates that the mechanism adds a plausible answer, highlighting the role of external forcing like ice melting in circulation and spring-summer heating changes over Europe (see **Supplementary Information; Extended Data Fig. 8**).

Two prevailing theoretical frameworks are commonly invoked to interpret summer dynamical circulation changes and surface extremes (**Coumou et al., 2018**), which form the context for this study. On the one hand, Arctic warming since 1979, though weaker in summer than in other seasons, still exceeds the global average by a factor of two (**Rantanen et al., 2022**), with strong reductions in sea-ice extent and snow cover (**Coumou et al., 2018**), a weakened meridional temperature gradient, upper-level zonal winds (**Francis and Vavrus, 2015**) and

weakening circulation and storms tracks (**Coumou et al., 2015; Chemke and Coumou, 2024**). These changes tend to enhance jet stream waviness as noted in some studies (**Francis and Vavrus, 2012; Trouet et al., 2018; Saurral et al. 2025**), though recent work finds that the strength—and even the direction—of the waviness response depends on the specific metric used (**Geen et al., 2023**). More broadly, the influence of the Arctic in the mid-latitude circulation remains debated (**Kang et al., 2023; Hassanzadeh et al., 2014; IPCC, 2021**), and there is little to no evidence on the role of Greenland melting on the jet stream variability. On the other hand, several recent summer HWs in the Northern Hemisphere midlatitudes have been linked to slow-moving, quasi-stationary planetary Rossby waves, often embedded in a circumglobal wave train (e.g., **Coumou et al., 2014**; **Kornhuber et al., 2019; Jiménez-Esteve et al. 2022**) and sometimes amplified via quasi-resonant amplification (QRA; **Petoukhov et al., 2013; Kornhuber et al., 2020**; **Mann et al., 2018; Mann et al., 2017).** While our results do not establish a direct correspondence with QRA, we do find connections with this broader framework, in the sense that the regional pattern underlying the proposed cascading mechanism is often embedded within a quasi-stationary wave-7 structure, suggesting potential linkages to hemispheric-scale dynamics (**see Supplementary Information**).

Our study shows that Greenland ice melt is not only a key driver of global sea-level rise, but also a major forcing factor behind hemispheric-scale circulation shifts with potential hazardous consequences. While the North Atlantic "cold blob" has been recognized as a likely fingerprint of this risk, here we show that Greenland melting initiates a previously unidentified cascading mechanism. This mechanism links oceanic changes to Euro-Mediterranean climate extremes and accelerated regional warming, including the deadly, record-breaking derecho convective storm in 2022. Our findings uncover the Euro-Mediterranean as a climate-change hotspot where dynamical circulation changes amplify dangerous phenomena. The analysis reveals critical cascading processes within the Earth system that must be adequately represented to capture potentially catastrophic socioeconomic, human and ecological impacts. Incorporating these processes is essential for improving forecasts systems, Earth system models, and long-term projections, and represents a major step towards effective early-warning and mitigation strategies.

Methods

ERA5 reanalysis: To analyze changes in the atmospheric circulation from an observational perspective, here we use ERA5 reanalysis (**Hersbach et al., 2020**). ERA5 has demonstrated to be the most reliable reanalysis dataset (**Horton, 2022**).

Group separation (HRA vs LRA): The two contrasting group behaviours are obtained based on the filtering of the 500 hPa zonal anomaly geopotential height (ZAGH) probability distribution over western Europe (**Fig. 2a**), in order to detect years with a completely different behaviour of the atmospheric circulation, compared to the climatology. Based on the shape of the distribution and its centroid, which is ~2.5 dam, group 1 is built by selecting the years where at least 3 of the 5 (≥60%) spring-summer seasonal months (April-August) have values above 5 dam. Note also that ~5 dam is where the 1993-2022 curve starts to surpass the 1950-1979 curve. On the other hand, for consistency, group 2 should be years where at least 3 of the 5 seasonal months are below 0 dam, but as only a few

years are retained we relaxed the filter for this group down to 2 of 5 (≥40%). Thus, group 1 corresponds to those years where the atmospheric circulation is associated with high activity of ridge persistence (HRA in the main text) over western Europe, where group 2 is consistent with low activity (LRA), absent, or even including above-normal trough activity. Note that this analysis aims at studying changes in persistence rather than merely changes in frequency. Graphic information of this group separation is provided in **Extended Data Fig. 2**.

Mass balance analysis: To estimate the surface freshening associated with the subpolar cold anomalies, we used a surface mass balance analysis. The idea behind the surface mass balance is to use the influence of freshwater on the SST to infer its variability. Any surface temperature decrease leads to a mass increase, since colder water is heavier than lighter water. Conservation of mass implies that this mass cannot be created by itself. It must be delivered to the region by advection, mixing / entrainment, or the surface fluxes. Thus, the objective of the mass balance analysis is to examine all possible sources of the increased mass associated with the negative SST anomaly.

Since the detailed derivation is lengthy and has already been detailed by earlier studies (**Oltmanns et al., 2020; 2024; under review**), we only provide the key result of the mass balance analysis here. In earlier studies, it was found that all possible sources, including the surface heat and buoyancy fluxes, were too small to account for the positive mass anomaly associated with the negative SST anomaly. In essence, the result states that there cannot be a positive mass anomaly, and the mass increase that is associated with negative SST anomaly must be balanced by a mass decrease associated with a negative salinity anomaly. In turn, this means that any SST anomalies in the subpolar North Atlantic in winter have been associated with density-compensating or nearly density-compensating salinity anomalies:

$$\alpha \cdot \Delta SST \approx \beta \cdot \Delta SSS$$

where α and β are the thermal and haline expansions coefficients respectively and ΔSST and ΔSSS refer to the SST and sea surface salinity anomalies, relative to the climatological mean. The uncertainties associated with the resulting salinity estimates were found to be approximately one order of magnitude smaller than the anomalies themselves (**Oltmanns et al., 2020; 2024; in revision**).

To estimate the freshwater differences between the HRA and LRA years, we carried out the surface mass balance for the composite difference SST anomalies in March and the cooling from the preceding autumm to March, associated with the HRA versus LRA years (**Fig. 4k and l**), using the ERA5 reanalysis to calculate the surface heat and buoyancy fluxes, vertical and horizontal Ekman transports. First, we observed that over the investigated period since 1950, there was a substantial surface warming trend, superimposed on the freshwater-induced cold anomalies. When evaluating the mass balances, we found that subtracting a regionally warming trend produces more accurate results. Thus, to account for the warming signal, we subtracted regionally averaged trends from all terms involved in the mass balance analysis, where the averaging was performed over the entire North Atlantic (20 N to 65 N). The results are not sensitive to the exact region as long as it is sufficiently large. Moreover, since the trend was not linear, we approximated it with a three-degree polynomial. Upon this lowpass filtering, we again found the uncertainties to be one order of magnitude smaller than the magnitude of the anomalies, amounting to about 4% in the 95% confidence regions (**Fig. 4m and n**), in good agreement with earlier studies (Oltmanns et al., 2020; **Oltmanns et al., 2024; under review**).

Greenland ice melting: To assess the link between the ridge building over western Europe and the runoff of Greenland meltwater, integrated over the full ice sheet and year, we use Greenland runoff data since 1950, obtained from the Greenland climate model MAR, forced by the ERA5 reanalysis

(**Fettweis, 2022**). Thus, we found that, in the years prior to HRA years, the runoff from Greenland was on average 81.6 Gt larger than prior to LRA years (p-value = 0.01, using the Rank Sum test).

There was one "double-event" over the investigated period, corresponding to two consecutive HRA years in 1992 and 1993. Closer inspection of the associated North Atlantic SST and freshening showed that the North Atlantic freshwater was not fully exported in 1992. Thus, the cold North Atlantic SST anomaly from 1992 remained until 1993. In order to not count this melt event twice, we excluded the 1993 HRA event from the Greenland melt analysis and only used the 1992 HRA event.

Climate model simulations: Numerical experiments were performed using the global model IFS, with the model version referred to as Cycle 48r1, which was used operationally at ECMWF between June 2023 and November 2024 (https://confluence.ecmwf.int/display/FCST/Implementation+of+IFS+Cycle+48r1). In these experiments, the global atmospheric model was forced by prescribed SSTs. The atmospheric resolution was 36 km with 137 vertical levels up to 0.01 hPa. The ensemble size was 25 members and the length of the forecast integrations was 5 months. We performed two main sets of experiments:

Analysis of the 2022 behaviour: Here the atmospheric model initialized on 1st May 2022 was forced with the 2022 observed SST pattern as boundary forcing, and compared to model forced by the climatological SSTs (ERA5; 1950-2022).

Analysis of the compositing behaviour of HRA and LRA years: Here we use the composite HRA SST pattern as forcing for the model and compare with the simulation using climatological SSTs and with the simulations using the composite SST pattern in LRA years. As the SSTs composites from HRA and LRA years are built from monthly data, we multiply this SST pattern by 4 in order to obtain more realistic daily SSTs anomalies, resulting in anomalies of the order of 1-2 ºC. The simulations are started at two initial times, 1st March and 1st May 2022, to study time-dependent predictability.

Atmospheric and marine heatwaves (HWs): The impact of the cascading mechanism on surface heatwaves is undertaken with two different metrics describing the HW activity. On one hand, atmospheric HWs are analysed with the Heat Wave Magnitude Index (HWMI), adapted from **Russo et al. (2015)**. This metric identifies heatwave events as periods of at least three consecutive days in which daily maximum 2 m temperature exceeds the local 90th percentile climatological threshold for that calendar day. For each event, the magnitude (M) is also calculated as the cumulative relative exceedance above the threshold:

$$M = \sum_{d=1}^{D} \frac{T(d) - T_{90}(d)}{T_{90}(d)}$$

where $T(d)$ is the daily maximum temperature on day d, $T_{90}(d)$ is the corresponding 90th percentile threshold, and D is the number of consecutive days in the event (with $D \geq 3$).

For each grid point and each summer season (June–July–August), we compute:

1. **Number of HW events (N_{HW}):** the total count of detected HW episodes.
2. **Cumulative HWMI (ΣM)**: the sum of magnitudes of all events, representing the seasonal severity of heatwaves.

This approach allows accounting for both changes in frequent but moderate events and fewer but more intense AHWs.

On the other hand, marine heatwaves (MHWs) are characterized following the framework of **Hobday et al. (2016)**. Daily sea surface temperature (SST) is compared against a seasonally varying baseline climatology, and MHWs are defined as periods of at least five consecutive days when SST exceeds the 90th percentile threshold for that calendar day. Each event is further classified into categories of increasing severity depending on the degree of exceedance above the threshold:

- **Category I (Moderate):** $T > T_{90}$
- **Category II (Strong):** $T > T_{90} + 1 \times (T_{99} - T_{90})$
- **Category III (Severe):** $T > T_{90} + 2 \times (T_{99} - T_{90})$
- **Category IV (Extreme):** $T > T_{90} + 3 \times (T_{99} - T_{90})$

where T_{90} and T_{99} are the 90th and 99th percentile climatological thresholds, respectively. This categorization allows not only the identification of the occurrence of MHWs but also the quantification of their intensity, enabling a consistent comparison across years.

Convective activity indexes: Different convective indexes are used (**Fig. 4g-j**) as environmental indicators for the potential of severe convective storms to produce impactful hazards like tornadoes, large hail and strong winds. These indexes are based on the study of **Taszarek et al. (2021).** These are the STP (Significant Tornado Parameter), DCP (Derecho Composite Parameter), SCP (Supercell Composite Parameter), HSI (Hail Size Index) and SHIP (Significant Hail Parameter). The convective environment indexes have been computed using the *thundeR* R package (**Taszarek et al. 2021**; https://github.com/bczernecki/thundeR).

Saharan air intrusions (SAIs): We identify the Saharan air masses through two indicators that try to capture the warmth and homogeneity of an air column at a specific grid point (**Sousa, et al., 2019; Cos, et al., 2025**). The first indicator is the geopotential thickness between 1000 and 500 hPa and, the second, the average potential temperature between 925 and 700 hPa. The thresholds that distinguish which values of each metric represent a mass of Saharan air are calculated from the spatial averages of the metrics over the Saharan region (box defined by 18ºN, 30°N, 9°W, 29° E) and rolling 31-day window climatologies (**Cos, et al., 2022**). This process provides thresholds for the two indicators for each day of the year. The points where the two thresholds are exceeded are identified as a Saharan air mass and, if more than 6% of the study area (box defined by, 35ºN, 44ºN, 10ºW, 6ºE) is occupied by such a mass, the day is considered a Saharan air intrusion (SAI). For these calculations, daily ERA5 temperature and geopotential averages are used in the different pressure levels. See **Extended Data Fig. 10a** for an example of intrusion on 04/05/2015 with the limits marked by green and pink curves.

CMIP6 model analysis: The analysis to understand if CMIP6 climate models are able to simulate the cascading mechanism is done through the verification of a similar changing behaviour in two periods associated with different forced climate context, i.e., preindustrial-like and ACC-forced-like. The comparison is based upon the historical runs (1851-2014) from (#53) models of this model intercomparison ensemble. We compare the periods 1985-2014 vs 1851-1879 for ZAGH monthly means from the models in the list provided at the end of this section. The analysis is done by performing the same calculation as in ERA5 (1950-1979 vs 1993-2022) in **Fig. 2a** but with the periods mentioned above.

Warm Conveyor Belt (WCB) activity proxy: The WCB proxy is built based on their physical behaviour. WCBs are strong, warm, and moist airflows that ascend along extratropical cyclones, typically originating from low levels in the warm sector. Then, WCB can be estimated using integrated vapor transport (IVT) and mid-level ascent. WCB proxy will thus indicate regions with ascending air motion within a high moisture advection plume. For simplicity, we use an IVT proxy which is calculated as follows:

$$IVT'(p) = q(p)\sqrt{u(p)^2 + v(p)^2}$$

where *q(p)* is the specific humidity at pressure level *p* [kg/kg], *u(p)*, *v(p)* are the horizontal wind components [m/s] and $\sqrt{u(p)^2 + v(p)^2}$ is the horizontal wind speed magnitude. Then we multiply it by vertical velocity and evaluate over the 700 hPa level:

$$WCB(p) = q(p)\sqrt{u(p)^2 + v(p)^2}\left(-w(p)\right)$$

where *ω(p)* is the vertical velocity in pressure coordinates [Pa/s]. Finally, we normalize the result to scale [0,1] for better interannual comparison. Thus, the WCB activity proxy results:

$$WCB_{700}^{norm} = \frac{q(700)\sqrt{u(700)^2 + v(700)^2}\left(-w(700)\right) - \min}{\max - \min}$$

Low-frequency wave-activity flux: The wave-activity flux (WAF) for quasi-stationary waves is diagnosed as in **Riboldi et al. (2023)**, following the definition of Takaya and Nakamura (1997) to which the interested reader is referred to. It is worth to precise here that the computation is based on 10-day averaged daily 250 hPa streamfunction anomalies, computed against the smoothed daily climatology of streamfunction, zonal and meridional wind at the same level. These assumptions indicate that the so-obtained WAF is apt to diagnose low-frequency Rossby wave patterns. Composites for MJJ are obtained by averaging daily WAF values, and standardized anomalies are obtained with respect to the so-obtained three-month (i.e., during MJJ) mean and standard deviation.

Recurrent Rossby wave packets: The presence of recurrent Rossby wave packets (RRWPs, **Röthlisberger et al. 2019**) is assessed using the methodology outlined in **Ali et al. (2021)**. First, the 6-hourly meridional wind at 250 hPa is meridionally averaged between 30°N and 60°N to obtain a Hovmoeller diagram $V(\lambda, t)$ with respect to longitude λ and time t. Secondly, a 14-day running average is applied to filter out the synoptic time scale and highlight persistent -or recurrent- flow features. Thirdly, a Fourier transform is then applied to the smoothed Hovmoeller diagram at each time step, yielding the Fourier coefficients $\hat{V}(k, t)$ where k stands for the zonal wavenumber. The recurrence metric $R(\lambda, t)$ is then obtained by inverting the Fourier transform and calculating the wave envelope amplitude corresponding only to the wave subset between k=4-15, thus retaining only the contribution of synoptic-scale waves to the time-filtered meridional wind. More details and the code to compute the metric *R* can be found in **Ali et al. (2021)**.

Euro Atlantic Wave-7 pattern and quasi-resonant wave amplification (QRA) frequencies: We compute the daily wave-7 pattern index (W7I) following the methodology described in **Drouard et al. (2019).** We first apply a Fourier decomposition of the weekly mean meridional wind at 250 hPa (V250) latitudinally averaged between 30ºN and 60ºN and retain the amplitude of zonal wavenumber 7. We then create a V250 composite of high amplitude events (weekly amplitudes > 1.5SD) for all weeks

composed between June and August. This composite is used to derive a daily index (W7I) by doing the spatial Spearman correlation of the V250 (smoothed prior to computation using a 7-day running mean) with this high-amplitude Wave-7 event composite over the midlatitudes of the Euro-Atlantic sector (37.5–57.5◦N, 30◦W-60◦E). Finally, the daily index is standardized again.

Data availability

Data that support the findings will be made available on reasonable request to the corresponding authors. Source data are freely available under ERA5 Copernicus server and the climate model simulations will be made available on reasonable request to the corresponding authors.

Code availability

Software and code routines developed for the data analysis will be made available on reasonable request to the corresponding authors.

References

Ballester, J. et al. Heat-related mortality in Europe during the summer of 2022. Nat. Med. 29, 1857–1866 (2023).

Battaglioli, F., Groenemeijer, P., Púčik, T., Taszarek, M., Ulbrich, U., & Rust, H. (2023). Modeled Multidecadal Trends of Lightning and (Very) Large Hail in Europe and North America (1950–2021). Journal of Applied Meteorology and Climatology, 62(11), 1627-1653.

Bischof, S., Pilch Kedzierski, R., Hänsch, M., Wahl, S., & Matthes, K. (2023). The role of the North Atlantic for heat wave characteristics in Europe, an ECHAM6 study. Geophysical Research Letters, 50, e2023GL105280. https://doi.org/10.1029/2023GL105280

Blackport, R., Screen, J.A. Weakened evidence for mid-latitude impacts of Arctic warming. Nat. Clim. Chang. 10, 1065–1066 (2020). https://doi.org/10.1038/s41558-020-00954-y

Caesar, L., Rahmstorf, S., Robinson, A. et al. Observed fingerprint of a weakening Atlantic Ocean overturning circulation. Nature 556, 191–196 (2018). https://doi.org/10.1038/s41586-018-0006-5

Christ, S., Wenta, M., Grams, C. M., and Oertel, A.: From sea to sky: understanding the sea surface temperature impact on an atmospheric blocking event using sensitivity experiments with the ICOsahedral Nonhydrostatic (ICON) model, Weather Clim. Dynam., 6, 17–42, https://doi.org/10.5194/wcd-6-17-2025, 2025.

Chemke, R., & Coumou, D. (2024). Human influence on the recent weakening of storm tracks in boreal summer. npj Climate and Atmospheric Science, 7(1), 86.

Chevuturi, A., Oltmanns, M., Tanguy, M. et al. Oceanic drivers of UK summer droughts.Commun Earth Environ 6, 437 (2025). https://doi.org/10.1038/s43247-025-02367-1

Cohen, J., Screen, J. A., Furtado, J. C., Barlow, M., Whittleston, D., Coumou, D., ... & Jones, J. (2014). Recent Arctic amplification and extreme mid-latitude weather. Nature geoscience, 7(9), 627-637.

Cohen, J., Zhang, X., Francis, J., Jung, T., Kwok, R., Overland, J., ... & Yoon, J. (2020). Divergent consensuses on Arctic amplification influence on midlatitude severe winter weather. Nature Climate Change, 10(1), 20-29.

Cos, P., Olmo, M., Campos, D., Marcos-Matamoros, R., Palma, L., Muñoz, Á. G., and Doblas-Reyes, F. J.: Saharan warm-air intrusions in the western Mediterranean: identification, impacts on temperature extremes, and large-scale mechanisms, Weather Clim. Dynam., 6, 609–626, https://doi.org/10.5194/wcd-6-609-2025, 2025.

Coumou, D., Petoukhov, V., Rahmstorf, S., Petri, S., & Schellnhuber, H. J. (2014). Quasi-resonant circulation regimes and hemispheric synchronization of extreme weather in boreal summer. Proceedings of the National Academy of Sciences, 111(34), 12331-12336.

Coumou, D., Lehmann, J., & Beckmann, J. (2015). The weakening summer circulation in the Northern Hemisphere mid-latitudes. Science, 348(6232), 324-327.

Coumou, D., Di Capua, G., Vavrus, S., Wang, L., & Wang, S. (2018). The influence of Arctic amplification on mid-latitude summer circulation. Nature Communications, 9(1), 2959.

D'Andrea, F., Duvel, J.-P., Rivière, G., Vautard, R., Cassou, C., Cattiaux, J., et al. (2024). Summer deep depressions increase over the Eastern North Atlantic. Geophysical Research Letters, 51, e2023GL104435. https://doi.org/10.1029/2023GL104435

Drouard, M., Kornhuber, K., & Woollings, T. (2019). Disentangling dynamic contributions to summer 2018 anomalous weather over Europe. Geophysical Research Letters, 46(21), 12537–12546. https://doi.org/10.1029/2019GL084601

Fan, Y., D. Chan, P. Zhang, and L. Li, 2024: Disagreement on the North Atlantic Cold Blob Formation Mechanisms among Climate Models. J. Climate, 37, 4061–4078, https://doi.org/10.1175/JCLI-D-23-0654.1.

Faranda, D., Pascale, S., & Bulut, B. (2023). Persistent anticyclonic conditions and climate change exacerbated the exceptional 2022 European-Mediterranean drought. Environmental Research Letters.

Fery, L. and Faranda, D, 2024.: Analysing 23 years of warm-season derechos in France: a climatology and investigation of synoptic and environmental changes, Weather Clim. Dynam., 5, 439–461, https://doi.org/10.5194/wcd-5-439-2024, 2024.

Francis, J. A., & Vavrus, S. J. (2015). Evidence for a wavier jet stream in response to rapid Arctic warming. Environmental Research Letters, 10(1), 014005.

Feser, F., L. van Garderen, and F. Hansen, 2024: The Summer Heatwave 2022 over Western Europe: An Attribution to Anthropogenic Climate Change. Bull. Amer. Meteor. Soc., 105, E2175–E2179, https://doi.org/10.1175/BAMS-D-24-0017.1.

Fettweis, Xavier. (2022). Modèle Atmosphérique Régional (MAR) version 3.11 regional climate model output, 1979-2019, Greenland domain, 10 kilometer (km) horizontal resolution. Arctic Data Center. doi:10.18739/A28G8FJ7F.

Garrido-Perez, J. M., Vicente-Serrano, S. M., Barriopedro, D., García-Herrera, R., Trigo, R., & Beguería, S. (2024). Examining the outstanding Euro-Mediterranean drought of 2021–2022 and its historical context. Journal of Hydrology, 630, 130653.

Garrabou, J., Gómez-Gras, D., Medrano, A., Cerrano, C., Ponti, M., Schlegel, R., Bensoussan, N., Turicchia, E., Sini, M., Gerovasileiou, V., Teixido, N., Mirasole, A., Tamburello, L., Cebrian, E., Rilov, G., Ledoux, J.-B., Souissi, J. B., Khamassi, F., Ghanem, R. … Harmelin, J.-G. (2022). Marine heatwaves drive recurrent mass mortalities in the Mediterranean Sea. Global Change Biology, 28, 5708–5725. https://doi.org/10.1111/gcb.16301

Geen, R., Thomson, S. I., Screen, J. A., Blackport, R., Lewis, N. T., Mudhar, R., et al. (2023). An explanation for the metric dependence of the midlatitude jet-waviness change in response to polar warming. Geophysical Research Letters, 50, e2023GL105132. https://doi.org/10.1029/2023GL105132

González-Alemán, J. J., Insua-Costa, D., Bazile, E., González-Herrero, S., Miglietta, M. M., Groenemeijer, P., & Donat, M. G. (2023). Anthropogenic warming had a crucial role in triggering the historic and destructive Mediterranean derecho in summer 2022. Bulletin of the American Meteorological Society, 104(8), E1526-E1532.

Grist, J. P., S. A. Josey, B. Sinha, J. A. Screen, R. Marsh, and D. Dey, 2025: The impact of a subpolar North Atlantic freshwater anomaly on Eurasian winter climate. J. Climate, https://doi.org/10.1175/JCLI-D-24-0669.1, in press.

Hanna E, Cappelen J, Fettweis X, et al. Greenland surface air temperature changes from 1981 to 2019 and implications for ice-sheet melt and mass-balance change. Int J Climatol. 2021; 41 (Suppl. 1): E1336–E1352. https://doi.org/10.1002/joc.6771

Hassanzadeh, P., Kuang, Z., & Farrell, B. F. (2014). Responses of midlatitude blocks and wave amplitude to changes in the meridional temperature gradient in an idealized dry GCM. Geophysical Research Letters, 41(14), 5223-5232.

Hoogewind, K. A., Baldwin, M. E., & Trapp, R. J. (2017). The impact of climate change on hazardous convective weather in the United States: Insight from high-resolution dynamical downscaling. Journal of Climate, 30(24), 10081–10100. https://doi.org/10.1175/JCLI-D-16-0885.1

Jackson, L. C., Alastrué de Asenjo, E., Bellomo, K., Danabasoglu, G., Haak, H., Hu, A., Jungclaus, J., Lee, W., Meccia, V. L., Saenko, O., Shao, A., and Swingedouw, D.: Understanding AMOC stability: the North Atlantic Hosing Model Intercomparison Project, Geosci. Model Dev., 16, 1975–1995, https://doi.org/10.5194/gmd-16-1975-2023, 2023.

Jiménez-Esteve, B., Kornhuber, K., & Domeisen, D. I. V. (2022). Heat extremes driven by amplification of phase-locked circumglobal waves forced by topography in an idealized atmospheric model. Geophysical Research Letters, 49, e2021GL096337. https://doi.org/10.1029/2021GL096337

Kang, J. M., Shaw, T. A., & Sun, L. (2023). Arctic sea ice loss weakens Northern Hemisphere summertime storminess but not until the late 21st century. Geophysical Research Letters, 50(9), e2022GL102301.

Kim, J. H., Nam, S. H., Kim, M. K., Serrano-Notivoli, R., & Tejedor, E. (2024). The 2022 record-high heat waves over southwestern Europe and their underlying mechanism. Weather and Climate Extremes, 46, 100729.

Kornhuber, K., Petoukhov, V., Petri, S., Rahmstorf, S., & Coumou, D. (2016). Evidence for wave resonance as a key mechanism for generating high-amplitude quasi-stationary waves in boreal summer. Climate Dynamics, 49, 1961-1979.

Kornhuber, K., Osprey, S., Coumou, D., Petri, S., Petoukhov, V., Rahmstorf, S., & Gray, L. (2019). Extreme weather events in early summer 2018 connected by a recurrent hemispheric wave-7 pattern. Environmental Research Letters, 14(5), 054002. https://doi.org/10.1088/1748-9326/ab13bf

Kornhuber, K., Osprey, S., Coumou, D., Petri, S., Petoukhov, V., Rahmstorf, S., & Gray, L. (2019). Extreme weather events in early summer 2018 connected by a recurrent hemispheric wave-7 pattern. Environmental Research Letters, 14(5), 054002.

Kornhuber, K., Coumou, D., Vogel, E., Lesk, C., Donges, J. F., Lehmann, J., & Horton, R. M. (2020). Amplified Rossby waves enhance risk of concurrent heatwaves in major breadbasket regions. Nature Research, 10(1), 48–53. https://doi.org/10.1038/s41558-019-0637-z

Kornhuber, K., Coumou, D., Vogel, E., Lesk, C., Donges, J. F., Lehmann, J., & Horton, R. M. (2020). Amplified Rossby waves enhance risk of concurrent heatwaves in major breadbasket regions. Nature Climate Change, 10(1), 48-53.

Kotz, M., Kuik, F., Lis, E., & Nickel, C. (2024). Global warming and heat extremes to enhance inflationary pressures. Communications Earth & Environment, 5(1), 116.

Lionello, P., D'Agostino, R., Ferreira, D., Nguyen, H., & Singh, M. S. (2024). The Hadley circulation in a changing climate. Ann NY Acad Sci., 1534, 69–93. https://doi.org/10.1111/nyas.15114

Li, J., Geiss, A., Feng, Z., Leung, L. R., Qian, Y., and Cui, W.: A derecho climatology (2004–2021) in the United States based on machine learning identification of bow echoes, Earth Syst. Sci. Data, 17, 3721–3740, https://doi.org/10.5194/essd-17-3721-2025, 2025.

Li X., M.E. Mann, M.F. Wehner, & S. Christiansen, Increased frequency of planetary wave resonance events over the past half-century, Proc. Natl. Acad. Sci. U.S.A. 122 (25) e2504482122, https://doi.org/10.1073/pnas.2504482122 (2025)

López, J. M., 2007: A Mediterranean derecho: Catalonia (Spain), 17th August 2003. Atmos. Res., 83, 272–283, https://doi.org/10.1016/j.atmosres.2005.08.008.

Ma, Q., Shi, X., Scholz, P., Sidorenko, D., Lohmann, G., and Ionita, M.: Revisiting climate impacts of an AMOC slowdown: dependence on freshwater locations in the North Atlantic.Sci. Adv.10,eadr3243(2024).DOI:10.1126/sciadv.adr3243

Mann, M. E., Rahmstorf, S., Kornhuber, K., Steinman, B. A., Miller, S. K., & Coumou, D. (2017). Influence of anthropogenic climate change on planetary wave resonance and extreme weather events. Scientific reports, 7(1), 45242.

Mann, M. E., Rahmstorf, S., Kornhuber, K., Steinman, B. A., Miller, S. K., Petri, S., & Coumou, D. (2018). Projected changes in persistent extreme summer weather events: The role of quasi-resonant amplification. Science advances, 4(10), eaat3272.

Martín, M. L., Calvo-Sancho, C., Taszarek, M., González-Alemán, J. J., Montoro-Mendoza, A., Díaz-Fernández, J., ... & Martín, Y. (2024). Major role of marine heatwave and anthropogenic climate change on a Giant hail Event in Spain. Geophysical Research Letters, 51(6), e2023GL107632.

Molteni, F., R. Buizza, T. N. Palmer, and T. Petroliagis, 1996: The ECMWF ensemble prediction system: Methodology and validation.Quarterly Journal of the Royal Meteorological Society, 122(529):73–119, https://doi.org/10.1002/qj.49712252905.

Moreno-Chamarro, E., Caron, L.-P., Loosveldt Tomas, S., Vegas-Regidor, J., Gutjahr, O., Moine, M.-P., Putrasahan, D., Roberts, C. D., Roberts, M. J., Senan, R., Terray, L., Tourigny, E., and Vidale, P. L.: Impact of increased resolution on long-standing biases in HighResMIP-PRIMAVERA climate models, Geosci. Model Dev., 15, 269–289, https://doi.org/10.5194/gmd-15-269-2022, 2022.

Nakamura, H., and J. M. Wallace, 1993: Synoptic Behavior of Baroclinic Eddies during the Blocking Onset. Mon. Wea. Rev., 121, 1892–1903, https://doi.org/10.1175/1520-0493(1993)121<1892:SBOBED>2.0.CO;2.

Nakamura, H., M. Nakamura, and J. L. Anderson, 1997: The Role of High- and Low-Frequency Dynamics in Blocking Formation. Mon. Wea. Rev., 125, 2074–2093, https://doi.org/10.1175/1520-0493(1997)125<2074:TROHAL>2.0.CO;2.

Oltmanns, M., Karstensen, J., Moore, G. W. K., & Josey, S. A. (2020). Rapid cooling and increased storminess triggered by freshwater in the North Atlantic. Geophysical Research Letters, 47, e2020GL087207. https://doi.org/10.1029/2020GL087207

Oltmanns, M., Holliday, N. P., Screen, J., Moat, B. I., Josey, S. A., Evans, D. G., & Bacon, S. (2024). European summer weather linked to North Atlantic freshwater anomalies in preceding years, Weather Clim. Dynam., 5, 109–132, https://doi.org/10.5194/wcd-5-109-2024

Oltmanns, M., Holliday, N. P., Moat, B., & Bacon, S. (under review). Questioning North Atlantic freshening as a driver of rapid climate change. Journal of Climate.

Pastor, F., Paredes-Fortuny, L. & Khodayar, S. Mediterranean marine heatwaves intensify in the presence of concurrent atmospheric heatwaves. Commun Earth Environ 5, 797 (2024). https://doi.org/10.1038/s43247-024-01982-8

Patterson, M., Befort, D. J., O'Reilly, C. H., & Weisheimer, A. (2024). Drivers of the ECMWF SEAS5 seasonal forecast for the hot and dry European summer of 2022. Quarterly Journal of the Royal Meteorological Society, 150(765), 4969-4986.

Petoukhov, V., Rahmstorf, S., Petri, S., & Schellnhuber, H. J. (2013). Quasiresonant amplification of planetary waves and recent Northern Hemi-sphere weather extremes. Proceedings of the National Academy of Sciences of the United States of America, 110(14), 5336–5341. https://doi.org/10.1073/pnas.1222000110

Pontes, G.M., Menviel, L. Weakening of the Atlantic Meridional Overturning Circulation driven by subarctic freshening since the mid-twentieth century. Nat. Geosci. 17, 1291–1298 (2024). https://doi.org/10.1038/s41561-024-01568-1

Priestley, M. D. K., & Catto, J. L. (2022). Improved representation of extratropical cyclone structure in HighResMIP models. Geophysical Research Letters, 49, e2021GL096708. https://doi.org/10.1029/2021GL096708

Priestley, M. D. K., D. Ackerley, J. L. Catto, K. I. Hodges, R. E. McDonald, and R. W. Lee, 2020: An Overview of the Extratropical Storm Tracks in CMIP6 Historical Simulations. J. Climate, 33, 6315–6343, https://doi.org/10.1175/JCLI-D-19-0928.1.

Rantanen, M., Karpechko, A. Y., Lipponen, A., Nordling, K., Hyvärinen, O., Ruosteenoja, K., ... & Laaksonen, A. (2022). The Arctic has warmed nearly four times faster than the globe since 1979. Communications earth & environment, 3(1), 168.

Roberts, M. J., Reed, K. A., Bao, Q., Barsugli, J. J., Camargo, S. J., Caron, L.-P., Chang, P., Chen, C.-T., Christensen, H. M., Danabasoglu, G., Frenger, I., Fučkar, N. S., Hasson, S. U., Hewitt, H. T., Huang, H., Kim, D., Kodama, C., Lai, M., Leung, L.-Y. R., Mizuta, R., Nobre, P., Ortega, P., Paquin, D., Roberts, C. D., Scoccimarro, E., Seddon, J., Treguier, A. M., Tu, C.-Y., Ullrich, P. A., Vidale, P. L., Wehner, M. F., Zarzycki, C. M., Zhang, B., Zhang, W., and Zhao, M.: High Resolution Model Intercomparison Project phase 2 (HighResMIP2) towards CMIP7, EGUsphere [preprint], https://doi.org/10.5194/egusphere-2024-2582, 2024.

Röthlisberger, M., L. Frossard, L. F. Bosart, D. Keyser, and O. Martius, 2019: Recurrent Synoptic-Scale Rossby Wave Patterns and Their Effect on the Persistence of Cold and Hot Spells. J. Climate, 32, 3207–3226, https://doi.org/10.1175/JCLI-D-18-0664.1.

Saurral, R. I., F. J. Doblas-Reyes, J. A. Screen, J. L. Catto, S. Hay, and H. Yu, 2025: Western Mediterranean Droughts Fostered by Arctic Sea Ice Loss. J. Climate, 38, 3005–3014, https://doi.org/10.1175/JCLI-D-25-0066.1.

Sánchez-Benítez, A., García-Herrera, R., Barriopedro, D., Sousa, P. M., & Trigo, R. M. (2018). June 2017: The earliest European summer mega-heatwave of reanalysis period. Geophysical Research Letters, 45, 1955–1962. https://doi.org/10.1002/2018GL077253

Schmidt, G. A., Mankoff, K. D., Bamber, J. L., Carroll, D., Chandler, D. M., Coulon, V., Davison, B. J., England, M. H., Holland, P. R., Jourdain, N. C., Li, Q., Marson, J. M., Mathiot, P., McMahon, C. R., Moon, T. A., Mottram, R., Nowicki, S., Olivé Abelló, A., Pauling, A. G., Rackow, T., and Ringeisen, D.: Datasets and protocols for including anomalous freshwater from melting ice sheets in climate simulations, EGUsphere [preprint], https://doi.org/10.5194/egusphere-2025-1940, 2025.

Screen, J. A., Deser, C., Smith, D. M., Zhang, X., Blackport, R., Kushner, P. J., ... & Sun, L. (2018). Consistency and discrepancy in the atmospheric response to Arctic sea-ice loss across climate models. Nature Geoscience, 11(3), 155-163.

Smith, D. M., Eade, R., Andrews, M. B., Ayres, H., Clark, A., Chripko, S., ... & Walsh, A. (2022). Robust but weak winter atmospheric circulation response to future Arctic sea ice loss. Nature communications, 13(1), 727.

Sousa P.M., Trigo R. M., Barriopedro D., Soares P. M. M., Santos J. A. (2018): European temperature responses to blocking and ridge regional patterns. Climate Dynamics, 50, 1-2, 457-477, doi: 10.1007/s00382-017-3620-2

Sousa, P. M., Barriopedro, D., Ramos, A. M., García-Herrera, R., Espírito-Santo, F., & Trigo, R. M. (2019). Saharan air intrusions as a relevant mechanism for Iberian heatwaves: The record breaking events of August 2018 and June 2019. Weather and Climate Extremes, 26, 100224.

Sousa P.M., Barriopedro D., García-Herrera R., Woollings T., Trigo R.M. (2021): A New Combined Detection Algorithm for Blocking and Subtropical Ridges. Journal of Climate, 34, 7735–7758. doi: 10.1175/JCLI-D-20-0658.1

Staten, P. W., J. Lu, K. M. Grise, S. M. Davis, and T. Birner, 2018: Reexamining tropical expansion. Nat. Climate Change, 8, 768–775, https://doi.org/10.1038/s41558-018-0246-2.

Steinfeld, D., Pfahl, S. The role of latent heating in atmospheric blocking dynamics: a global climatology. Clim Dyn 53, 6159–6180 (2019). https://doi.org/10.1007/s00382-019-04919-6

Surowiecki, A., N. Pilguj, M. Taszarek, K. Piasecki, T. Púčik, and H. E. Brooks, 2024: Quasi-Linear Convective Systems and Derechos across Europe: Climatology, Accompanying Hazards, and Societal Impacts. Bull. Amer. Meteor. Soc., 105, E1619–E1643, https://doi.org/10.1175/BAMS-D-23-0257.1.

Taszarek, M., Pilguj, N., Allen, J. T., Gensini, V., Brooks, H. E., & Szuster, P. (2021). Comparison of convective parameters derived from ERA5 and MERRA-2 with rawinsonde data over Europe and North America. Journal of Climate, 34(8), 3211-3237.

Torralba, V., Materia, S., Cavicchia, L., Álvarez-Castro, M. C., Prodhomme, C., McAdam, R., ... & Gualdi, S. (2024). Nighttime heat waves in the Euro-Mediterranean region: definition, characterisation, and seasonal prediction. Environmental Research Letters, 19(3), 034001.

Trigo, R. M., Barriopedro, D., Garrido-Perez, J. M., Simon, A., Plecha, S. M., Teles-Machado, A., ... & Garcia-Herrera, R. (2025). The outstanding European and Mediterranean heatwave activity during summer 2022. Atmospheric Research, 323, 108195.

Trouet, V., Babst, F., & Meko, M. (2018). Recent enhanced high-summer North Atlantic Jet variability emerges from three-century context. Nature communications, 9(1), 180.

Välisuo, I., Vihma, T., Pirazzini, R., & Schäfer, M. (2018). Interannual variability of atmospheric conditions and surface melt in Greenland in 2000–2014. Journal of Geophysical Research: Atmospheres, 123, 10,443–10,463. https://doi.org/10.1029/2018JD028445

van Westen, R. M. and Dijkstra, H. A.: Persistent climate model biases in the Atlantic Ocean's freshwater transport, Ocean Sci., 20, 549–567, https://doi.org/10.5194/os-20-549-2024, 2024.

Wandel, J., Büeler, D., Knippertz, P., Quinting, J. F., & Grams, C. M. (2024). Why moist dynamic processes matter for the sub-seasonal prediction of atmospheric blocking over Europe. Journal of Geophysical Research: Atmospheres, 129, e2023JD039791. https://doi.org/10.1029/2023JD039791

Yin, Z., Dong, B., Wei, W., & Yang, S. (2024). Anthropogenic impacts on amplified midlatitude European summer warming and rapid increase of heatwaves in recent decades. Geophysical Research Letters, 51, e2024GL108982. https://doi.org/10.1029/2024GL108982

Zhang, Q.L., Ding, M.H., van den Broeke, M.R., Noël, B., Fettweis, X., Wang, S., Sun, W.J., You, Q.L., Xiao, C.D., Qin, D.H. and Huai, B.J., 2025. Variations in Greenland surface melt and extreme events from 1958 to 2023. Advances in Climate Change Research. https://doi.org/10.1016/j.accre.2025.05.004.

Acknowledgments

J.J.G.A. thanks support from AEMET and from the Spanish PID2023-146344OB-I00 project, funded by MICIU/AEI/10.13039/501100011033 and by FEDER, EU.
C.C.S. the grant supported by the Spanish Ministerio de Ciencia, Innovación y Universidades (PRE2020-092343) and support from the GVA. PROMETEO Grant CIPROM/2023/38; and CSIC-LINCGLOBAL Ref. LINCG24042.
M.O. acknowledges support from the NERC grants CANARI (NE/W004984/1) and DIMSUM (NE/Y005090/1).
M.G.D. is grateful for support by the Horizon Europe project EXPECT (Grant 101137656).
D.B and B.J.E. acknowledge support from the the Ministry for the Ecological Transition and the Demographic Challenge (MITECO) and the European Commission NextGenerationEU (Regulation EU 2020/2094), through CSIC's Interdisciplinary Thematic Platform Clima (PTI-Clima).

Author information

Authors and Affiliations

AEMET/Spanish State Meteorological Agency, Madrid, Spain
Juan Jesus Gonzalez-Aleman

Alfred Wegener Institute, Germany
Marilena Oltmanns

University of Bremen, Germany
Marilena Oltmanns

National Oceanography Centre, Germany
Marilena Oltmanns

WSL Institute for the Snow and Avalanche Research (SLF), Switzerland
Sergi González-Herrero

European Centre for Medium-Range Weather Forecasts, United Kingdom
Frédéric Vitart

Barcelona Supercomputing Centre, Barcelona, Spain
Markus G. Donat & Francisco Doblas-Reyes & Pep Cos

Catalan Institution for Research and Advanced Studies (ICREA), Barcelona, Spain
Markus G. Donat & Francisco Doblas-Reyes

Instituto de Geociencias (IGEO), Consejo Superior de Investigaciones Científicas - Universidad Complutense de Madrid (CSIC - UCM), Madrid, Spain
David Barriopedro & Bernat Jiménez-Esteve

Institute for Atmospheric and Climate Science, ETH Zurich, Zurich, Switzerland
Jacopo Riboldi

Centro de Investigaciones sobre Desertificación, Consejo Superior de Investigaciones Científicas (CIDE, CSIC-UV-GVA), Climate, Atmosphere and Ocean Laboratory (Climatoc-Lab), Moncada, Valencia, Spain
Carlos Calvo-Sancho

Applied Mathematics and Computational Science Division, Lawrence Berkeley National Laboratory, Berkeley, California 94720 USA
Michael Wehner

Contributions

J.J.G.A conceived the study and designed the initial research; J.J.G.A did and oriented the research with inputs from S.G.H., M.G.D., F.D.R. and M.F.W., carried out the main calculations, prepared the figures and wrote the manuscript with the help of S.G.H., D.B. and M.O., and inputs from all the authors; M.O. developed and provided the mass balance and Greenland melting analysis; S.G.H. provided the CMIP6 data. F.V. performed the IFS ensemble model simulations. D.B. provided the subtropical ridge and blocking analysis. J.R. provided the Rossby wave dynamics analysis. C.C.S. calculated the convective indexes and performed the analysis. B.J.E. provided the IW7 and QRA analysis. P.C. provided the SAIs analysis. Finally, all authors revised the manuscript and provided feedback.

Corresponding authors

Correspondence to Juan Jesús González Alemán.

Ethics declarations

The authors declare no competing interests.

Extended data figures and tables

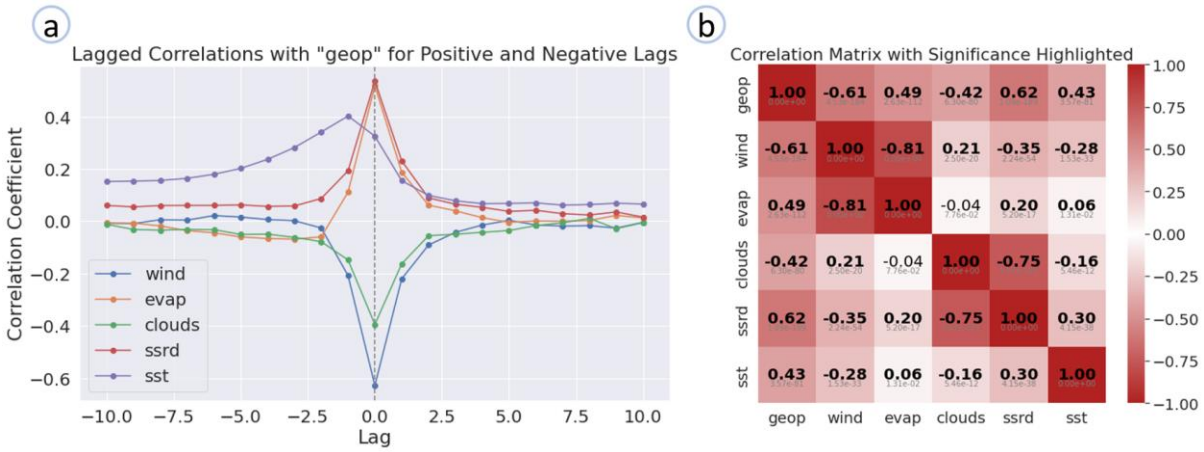

Extended Data Fig. 1: Climatological links between Europe GH and the SSTs over the western Mediterranean. (a) Lagged Pearson's correlation between the daily variability (from April to August) of the mean the geopotential height at 500 hPa over the green box in Figure 1a) and the surface wind (wind), surface evaporation (evap), cloud cover (clouds), surface incoming solar radiation (ssrd) and sea surface temperature (sst) over the western Mediterranean Sea (green box in Figure 1b). (b) Pearson's correlation matrix between the daily variability (from April to August) of all the six parameters in (a) and over the same box. Data from ERA5 reanalysis. The correlation is after detrending the data.

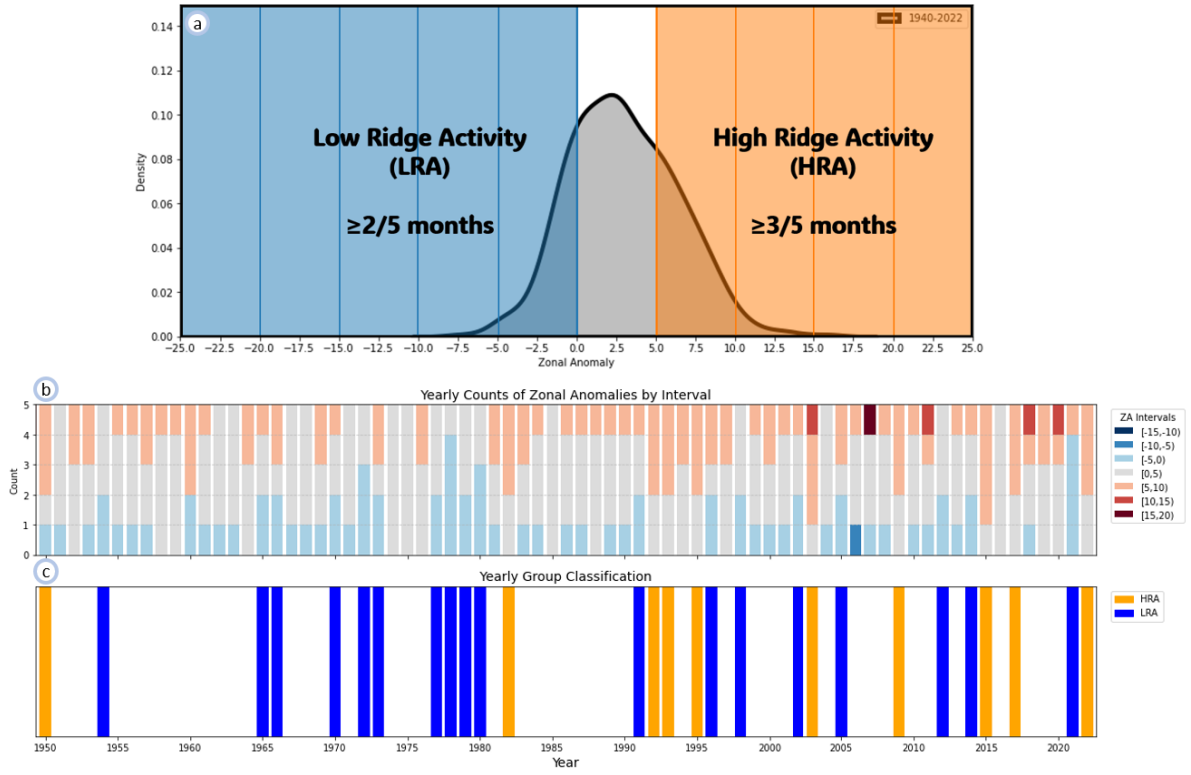

Extended Data Fig. 2: Graphical description of the group separation (HRA vs LRA years). (a) Probability density function of monthly mean ZAGH over the yellow box in **Figure 1a** in the period 1950-2022, and the partition of interval segments to define the group separation. (a) Yearly counts of the number of months per year at each interval of the ZAGH values in (a). (b) Group assignment per year in the 1950-2022 period. Data from ERA5 reanalysis.

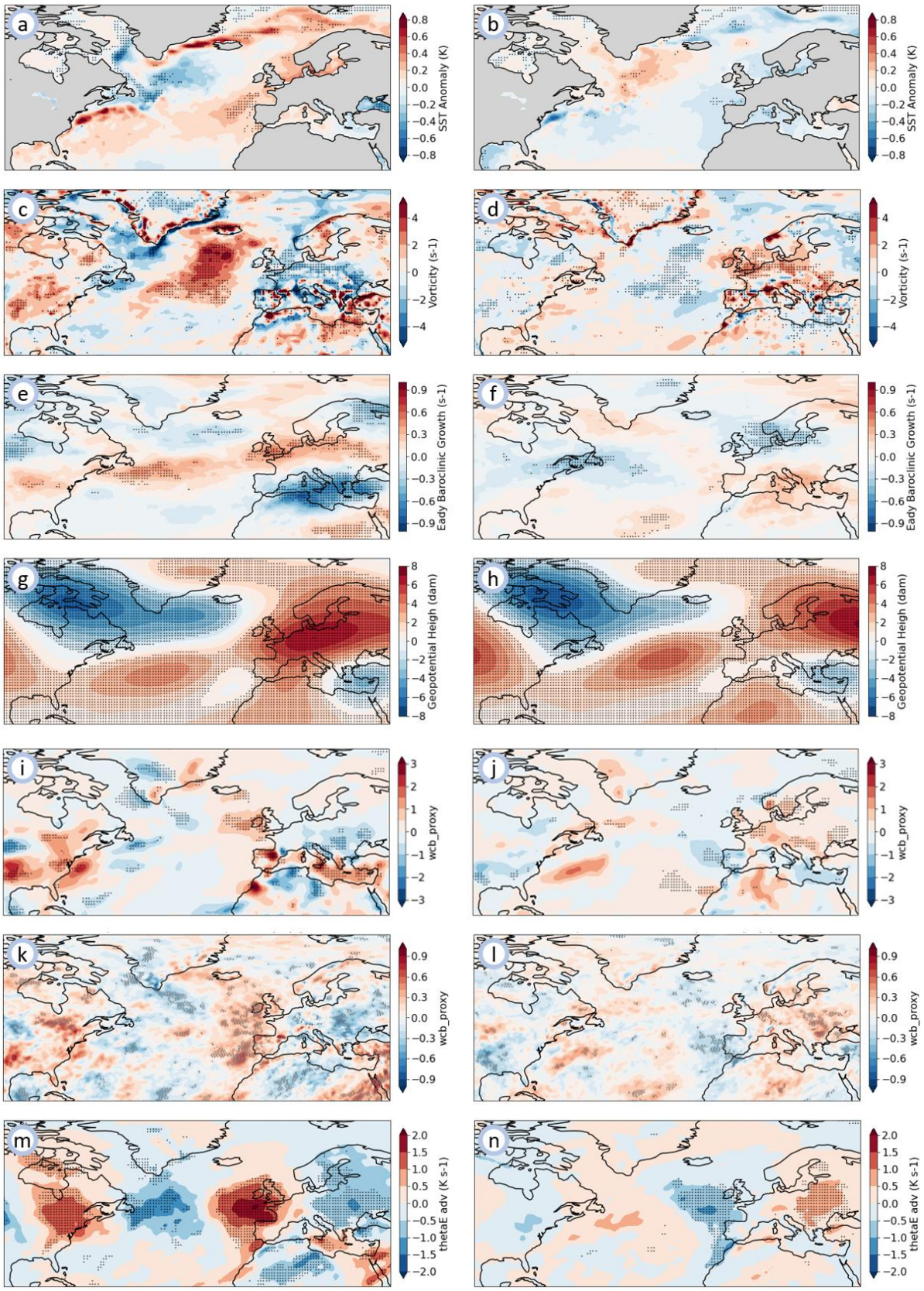

Extended Data Fig. 3. Significance analysis for the fields shown in Figure 3. (a-b) MJJ sea surface temperature for (a) HRA and (b) LRA years. (c-d) Same as (a-b) but for 850 hPa vorticity (s^{-1}). (e-f) Same as (a-b) but for Eady baroclinic growth (EBG; contours; interval 0.1x10^{1} s^{-1}). (g-h) Same as

(a-b) but for ZAGH (contours; interval 2 dam). (i-j) Same as (a-b) but for WCB activity proxy. (l-m) Same as (a-b) but for 850-hPa equivalent potential temperature advection ($0.5\text{x}10^5\ K\ s^{-1}$). (m-n) Same as (a-b) but for upper-level (150-300 hPa) divergence ($0.25\text{x}10^6\ s^{-1}$).

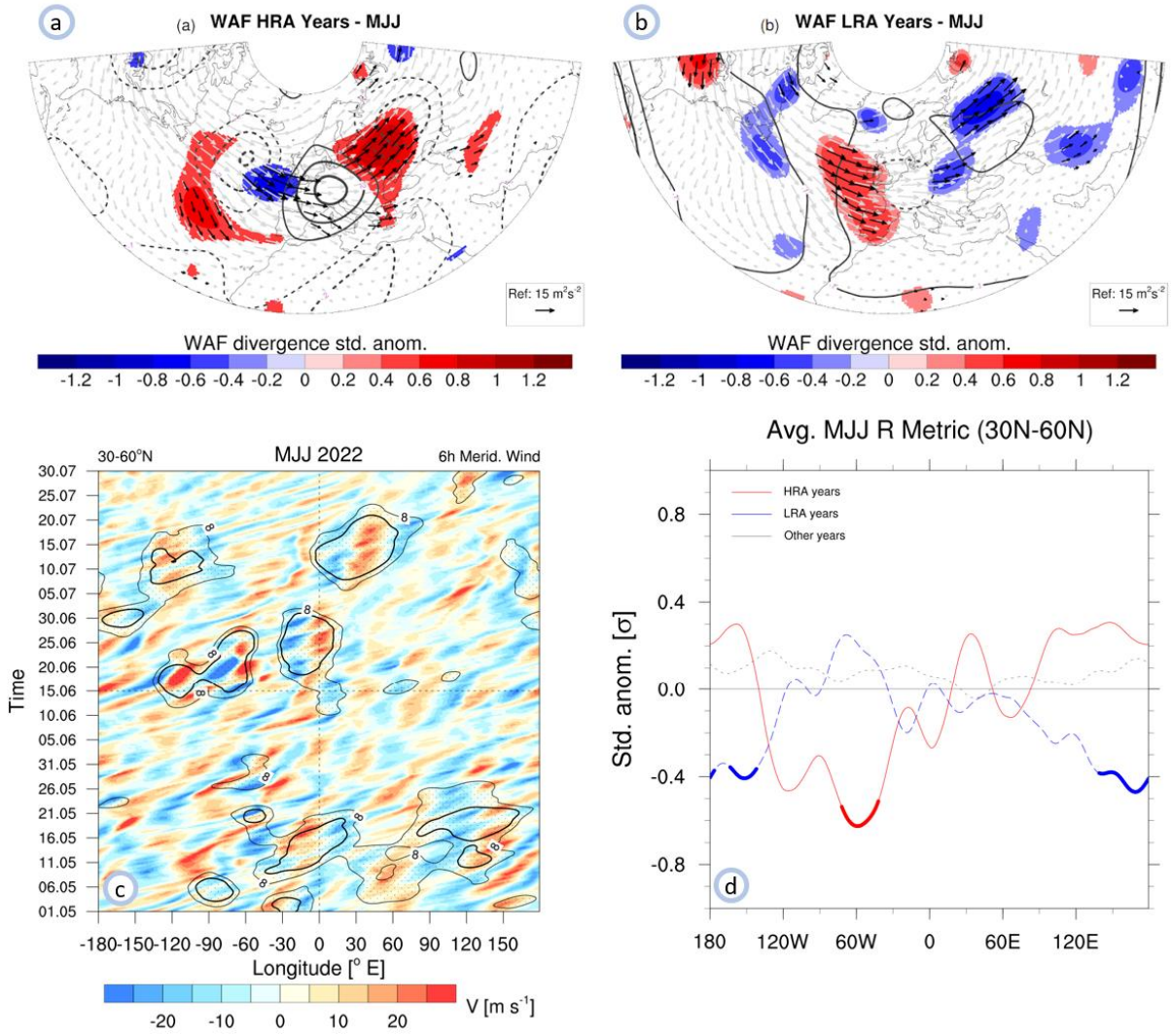

Extended Data Fig. 4: Properties of Rossby waves involved in the "atmospheric bridge". Composites of three-month averaged phase-independent WAF (arrows) and of its anomalous divergence (shaded) over the North Atlantic and Eurasian sector for (a) HRA years and (b) LRA years. Arrows are shown when their magnitude exceeds the 95th percentile or is below the 5th percentile of the corresponding randomly resampled distribution with respect to climatology (1500 iterations), and the same procedure is followed for WAF divergence anomalies. Standardized streamfunction anomalies are overlaid (black contours, dashed when negative, only ±0.1, 0.2 and 0.3σ). (c) Hovmoeller diagram for MJJ 2022 based on 6-hourly wind at 250hPa (shaded). Overlaid is the corresponding $R(\lambda, t)$ (black contours, only contours corresponding to 6 m/s and 8 m/s values). (d) Composite standardized anomalies of $R(\lambda, t)$ for HRA years (red), LRA years (blue) and other (non-HRA and non-LRA) years (grey). Lines are bold when anomalies are statistically significant (i.e., below the 2.5th or above the 97.5th percentile) after a random resampling with respect to climatology (2500 iterations).

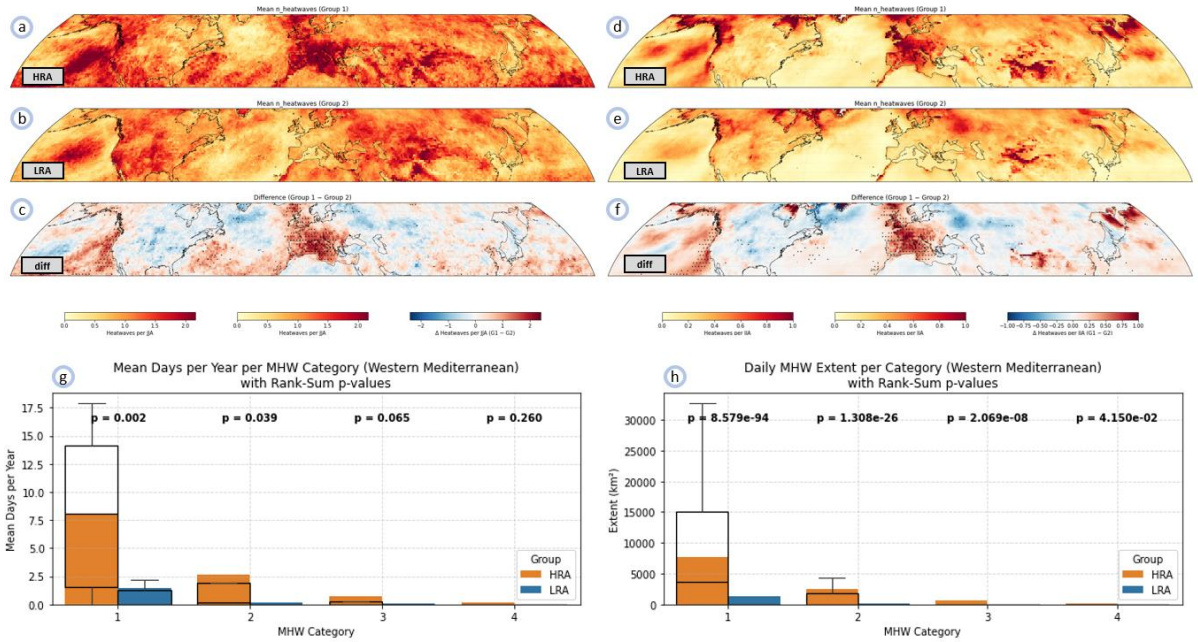

Extended Data Fig. 5: Surface impacts of the European persistent atmospheric circulation in terms of atmospheric and marine heatwaves. (a-c) Mean number of atmospheric heatwaves, defined with the HWMI, in (a) HRA years, (b) LRA years and (c) HRA-LRA differences. (d-f) Same as (a-c) but with the magnitude of the heatwaves. (g) Mean days (bars; at least over one grid box) per year of each marine heatwave category over the western Mediterranean (green box in Figure 1b) in HRA and LRA years. Overlaid is the boxplot of the yearly distribution. (h) The same information provided in (g) but for the mean extent (km2).

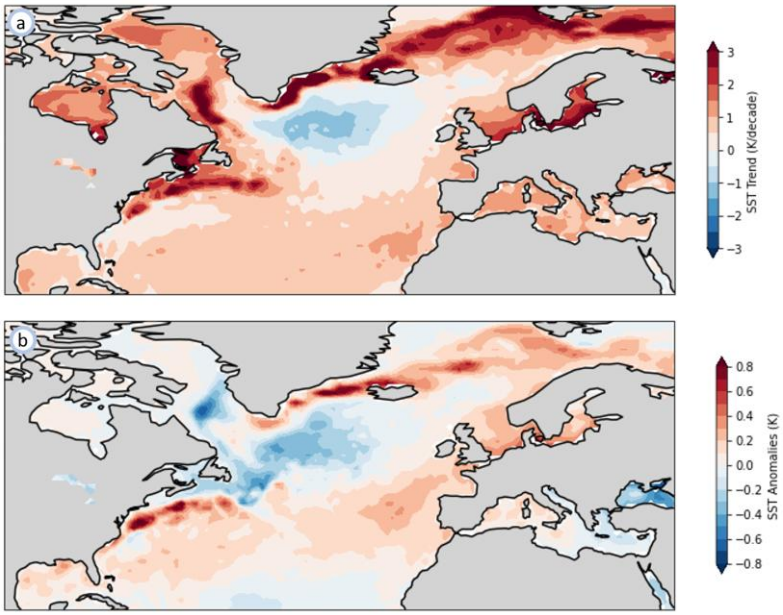

Extended Data Fig. 6: The North Atlantic warming hole, or cold blob, resembles the SST pattern in HRA years. (a) Decadal trend (K/decade) of the sea surface temperature in the period 1979-2022. (b) Sea surface temperature anomaly (K) composite (1950-2022) for HRA years in MJJ.

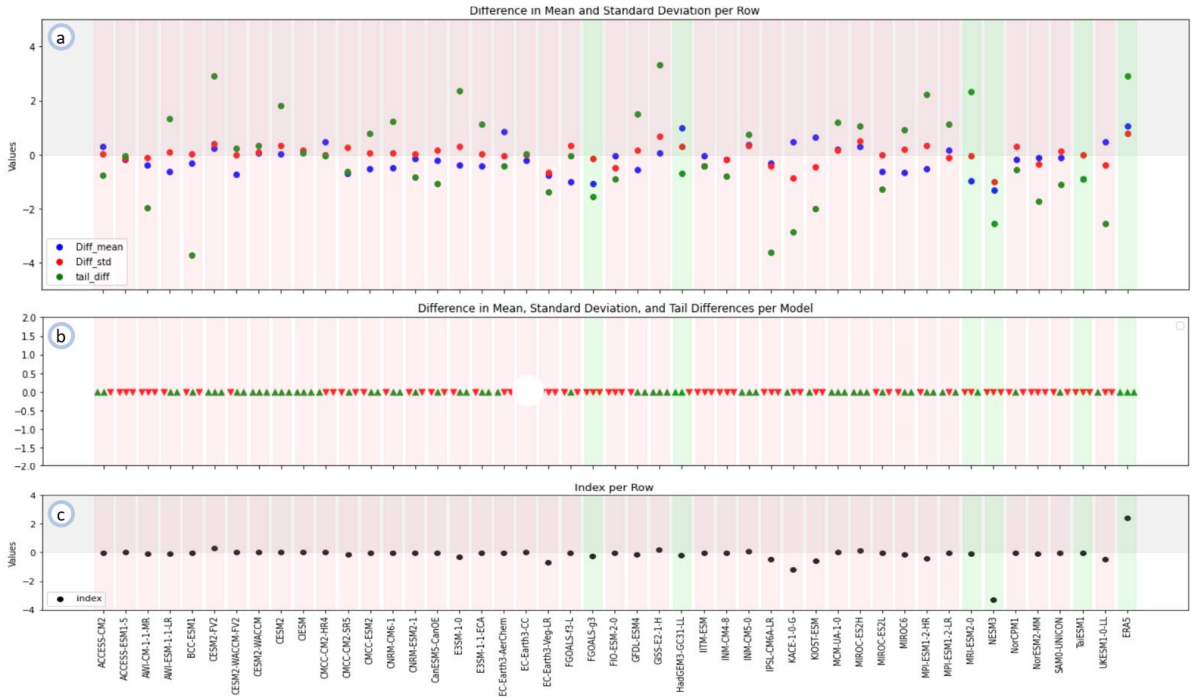

Extended Data Fig. 7: CMIP6 model simulations do not reproduce the cascading mechanism. (a) Values for the three metrics used (mean, standard deviation and tail differences) in the CMIP6 model assessment and comparison with ERA5. (b) Same information as in (a) but with symbols indicating the sign of the three metrics for better comparison analysis. (c) The same as (a) and (b) but in terms of the Shape Index.

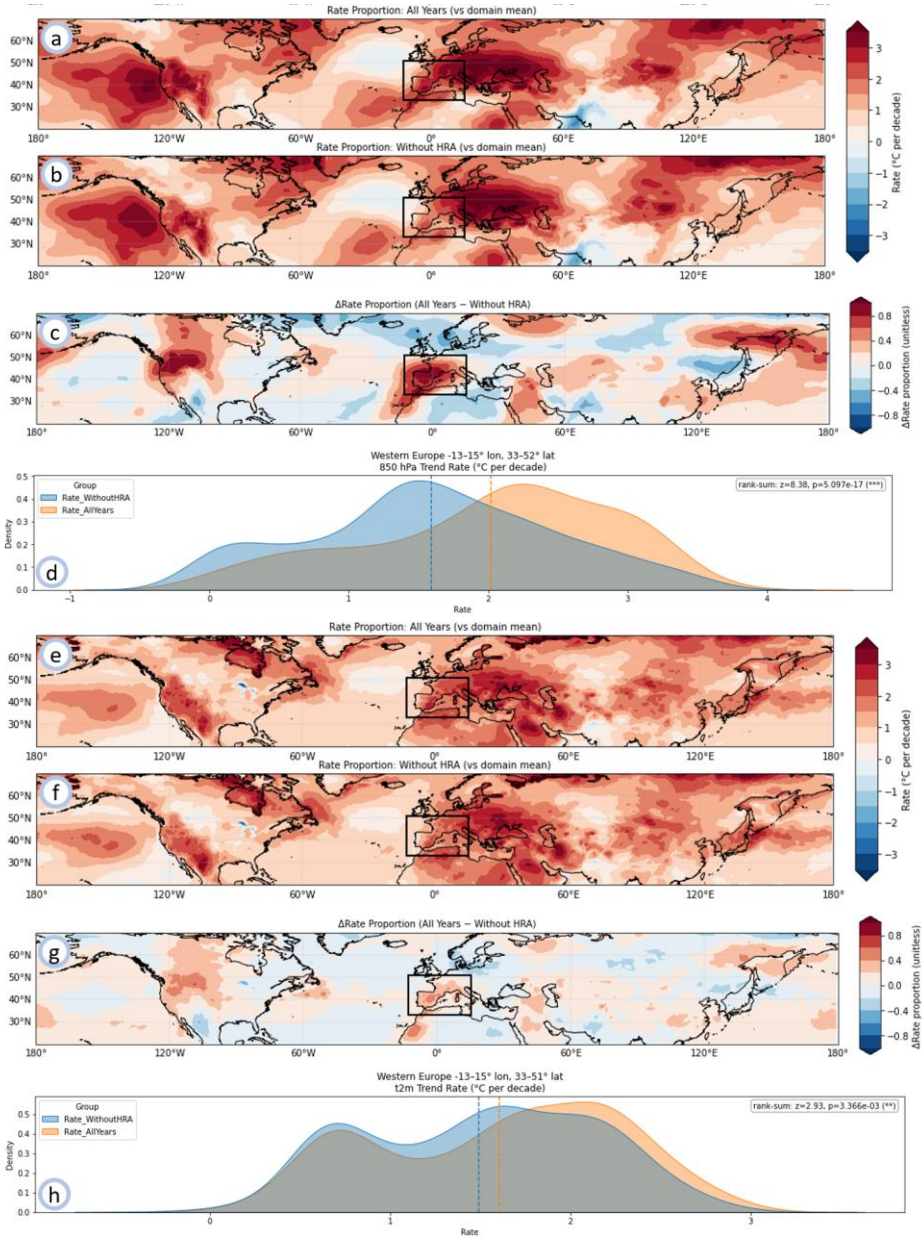

Extended Data Fig. 8: Influence of the cascading mechanism on the recent accelerated Europe warming. (a-d) Differential (rate, with respect to global) decadal trend of the temperature at 850 hPa in the period 1979-2022 considering (a) all years (b) all years minus HRA years, (c) differences between (b) and (a) and (d) the probability distribution functions for both cases over the black box in (a-b). (e-h) Same as (a-d) but for 2-meter temperature.

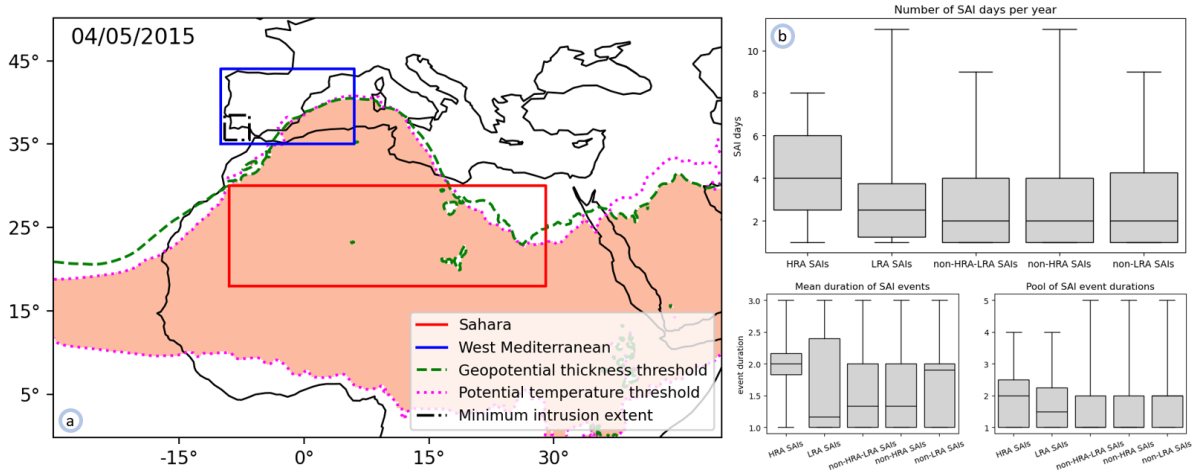

Extended Data Fig. 9: Saharan air intrusions (SAIs) are more frequent and long-lasting in HRA years. (a) Description of the main location of the regions analyzed and the characterization of the Saharan airmass and intrusions as in **Cos et al. (2025)**. (b-d) Amount of (b) intrusion days over the western Mediterranean (blue box), (c) mean duration of intrusion events and (d) pool of duration of intrusion events.

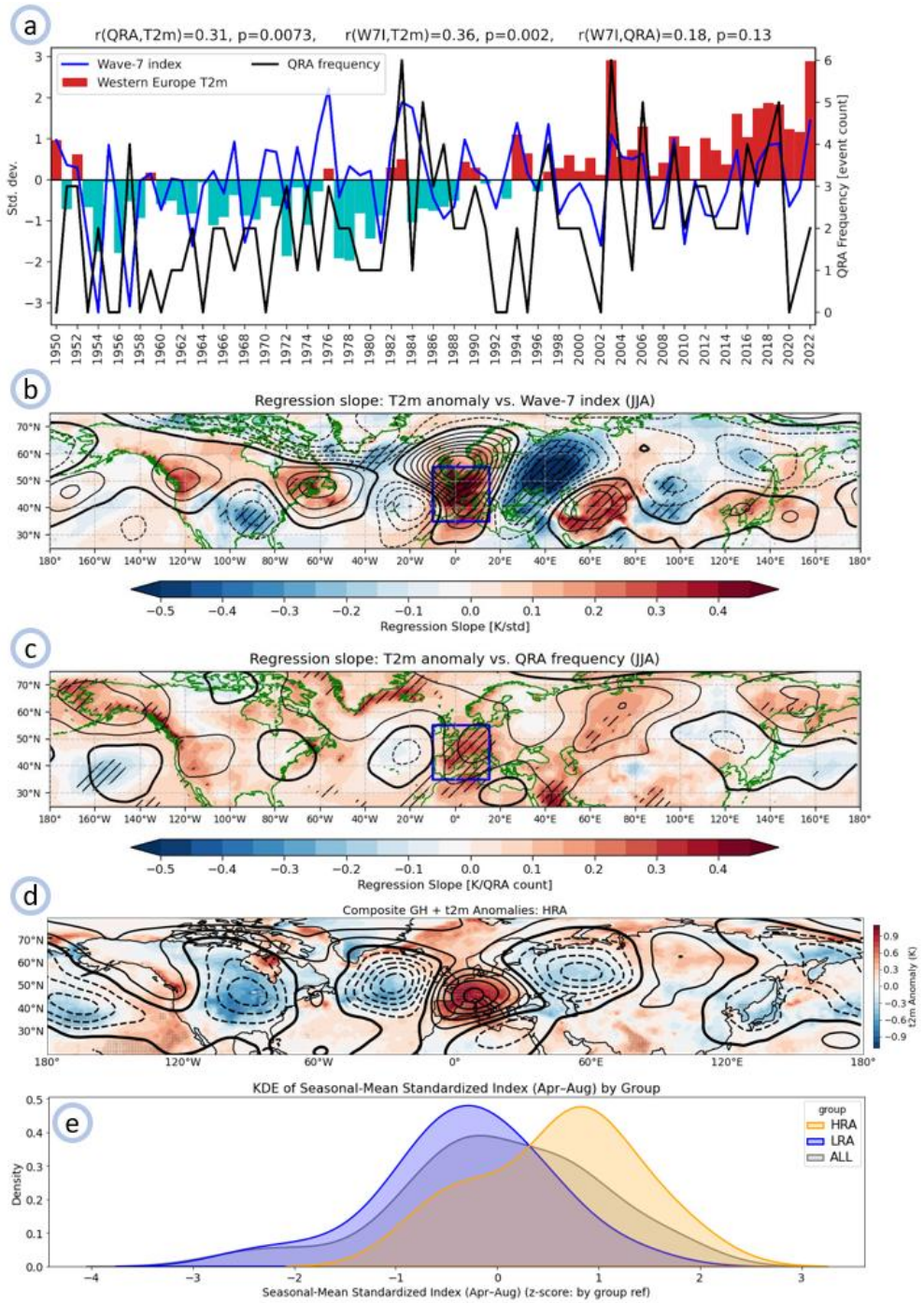

Extended Data Fig. 10: Links between the cascading mechanism and global planetary wave patterns. (a) Time series of the June–July–August (JJA) standardized W7I (blue), QRA frequency (black, from Li et al. 2025), and standardized Western European area-averaged 2 m temperature (bars). Western Europe is defined as the region outlined by the black box in (b,c). Correlation coefficients and corresponding *p*-values among the three indices are shown at the top. (b) Regression slopes between standardized W7I and JJA 2-m temperature (shading) and 500-hPa geopotential height (contours), and (c) between QRA frequency and JJA 2 m temperature (shading) and 500-hPa geopotential height (contours). Stippling in (b,c) and dots in (d) indicates significance at the 95% confidence level. (d) JJA 2-m temperature (shading) and 500-hPa geopotential height (contours) composite for HRA years. (e) Probability distribution functions of the W7I index associated with each group years (HRA vs LRA vs CLIM group).